

Production of $\Upsilon(nS)$ mesons in Pb + Pb and pp collisions at 5.02 TeV

G. Aad *et al.**
(ATLAS Collaboration)



(Received 9 May 2022; accepted 24 October 2022; published 22 May 2023)

A measurement of the production of vector bottomonium states, $\Upsilon(1S)$, $\Upsilon(2S)$, and $\Upsilon(3S)$, in Pb + Pb and pp collisions at a center-of-mass energy per nucleon pair of 5.02 TeV is presented. The data correspond to integrated luminosities of 1.38 nb^{-1} of Pb + Pb data collected in 2018, 0.44 nb^{-1} of Pb + Pb data collected in 2015, and 0.26 fb^{-1} of pp data collected in 2017 by the ATLAS detector at the Large Hadron Collider. The measurements are performed in the dimuon decay channel for transverse momentum $p_T^{\mu\mu} < 30 \text{ GeV}$, absolute rapidity $|y^{\mu\mu}| < 1.5$, and Pb + Pb event centrality 0–80%. The production rates of the three bottomonium states in Pb + Pb collisions are compared with those in pp collisions to extract the nuclear modification factors as functions of event centrality, $p_T^{\mu\mu}$, and $|y^{\mu\mu}|$. In addition, the suppression of the excited states relative to the ground state is studied. The results are compared with theoretical model calculations.

DOI: [10.1103/PhysRevC.107.054912](https://doi.org/10.1103/PhysRevC.107.054912)

I. INTRODUCTION

Quantum chromodynamics (QCD) predicts that at high temperatures and energy densities, hadronic matter undergoes a phase transition and turns into a state of deconfined quarks and gluons known as quark-gluon plasma (QGP). This state of matter is typically thought to be created in the collisions of two heavy nuclei at ultrarelativistic energies. In such collisions, heavy-flavor quarks, especially charm and bottom, are produced at an early stage in hard scattering processes and hence can probe QGP over its full evolution.

Formation of the QGP and the consequent modification to the heavy-quark potential are expected to lead to different quarkonium states dissolving at different temperatures of the medium [1]. This effect is known as sequential suppression [2]. While the excited states are dissociated just above the transition temperature $T_c \approx 155 \text{ MeV}$ needed to form the QGP, the ground states melt far above that value, creating a hierarchy in the measured suppression of quarkonium states. In particular, in Ref. [3], lattice calculations for the temperature-dependent behavior of the heavy-quark potential in full QCD theory were used to estimate the order of the suppression steps as functions of temperature and energy density. It was found that the $\Upsilon(1S)$ persists well above T_c , while $\Upsilon(2S)$ dissociates at about $1.1 T_c$ and $\Upsilon(3S)$ cannot exist at temperatures above T_c . Since then, quarkonium production and propagation through QGP have been extensively studied theoretically. Comprehensive reviews can be found in Refs. [4,5].

Quarkonia dissociation in QGP can happen along with recombination of uncorrelated heavy quarks [6–8], which in-

creases quarkonia yields. In this regard, it is interesting to compare bottomonium [$\Upsilon(1S)$, $\Upsilon(2S)$, $\Upsilon(3S)$, χ_b , etc.] to the charmonium family [J/ψ , $\psi(2S)$, χ_c , etc.], since recombination is expected to be much larger for the latter.

Experimentally, quarkonium suppression in nucleus-nucleus collisions has been studied extensively for both the bottomonia [9–16] and charmonia [17–23] families at Relativistic Heavy Ion Collider (RHIC) and Large Hadron Collider (LHC) energies. These measurements show strong suppression of quarkonia in nucleus-nucleus collisions compared to pp collisions, increasing for more central events, as well as stronger suppression of the excited Upsilon states [$\Upsilon(2S)$ and $\Upsilon(3S)$] relative to the ground state [$\Upsilon(1S)$].

In this paper, $\Upsilon(nS)$ production in pp and Pb+Pb collisions at $\sqrt{s} = 5.02 \text{ TeV}$ per nucleon-nucleon pair is studied as a function of transverse momentum ($p_T^{\mu\mu}$), rapidity, and Pb+Pb collision centrality.

II. THE ATLAS DETECTOR

The ATLAS detector [24] at the LHC covers nearly the entire solid angle around the collision point.¹ It consists of an inner tracking detector surrounded by a thin superconducting solenoid, electromagnetic and hadronic calorimeters, and a muon spectrometer incorporating three large superconducting air-core toroidal magnets.

The inner-detector (ID) system is immersed in a 2-T axial magnetic field and provides charged-particle tracking in

¹ATLAS uses a right-handed coordinate system with its origin at the nominal interaction point (IP) in the center of the detector and the z axis along the beam pipe. The x axis points from the IP to the center of the LHC ring, and the y axis points upward. Cylindrical coordinates (r, ϕ) are used in the transverse plane, ϕ being the azimuthal angle around the z axis. The pseudorapidity is defined in terms of the polar angle θ as $\eta = -\ln \tan(\theta/2)$, and the rapidity is defined as $y = (1/2)[\ln(E + p_z)/(E - p_z)]$.

*Full author list given at the end of the article.

Published by the American Physical Society under the terms of the [Creative Commons Attribution 4.0 International](https://creativecommons.org/licenses/by/4.0/) license. Further distribution of this work must maintain attribution to the author(s) and the published article's title, journal citation, and DOI.

the range $|\eta| < 2.5$. The high-granularity silicon pixel detector covers the vertex region and typically provides four measurements per track, the first hit normally being in the insertable B layer installed before run 2 [25,26]. It is followed by the silicon microstrip tracker, which usually provides eight measurements per track. These silicon detectors are complemented by the transition radiation tracker (TRT), which enables radially extended track reconstruction up to $|\eta| = 2.0$.

The muon spectrometer (MS) comprises separate trigger and high-precision tracking chambers measuring the deflection of muons in a magnetic field generated by the superconducting air-core toroids. The field integral of the toroids ranges between 2.0 and 6.0 Tm across most of the detectors. A set of precision chambers covers the region $|\eta| < 2.7$ with three layers of monitored drift tubes, complemented by cathode strip chambers in the forward region, where the background is highest. Resistive plate chambers (RPCs) and thin gap chambers (TGCs) with a coarse position resolution but a fast response time are used primarily to trigger on muons in the ranges $|\eta| < 1.05$ and $1.05 < |\eta| < 2.4$, respectively.

The zero-degree calorimeters (ZDCs) are located symmetrically at $z = \pm 140$ m and cover $|\eta| > 8.3$. The ZDCs use tungsten plates as absorbers, and quartz rods sandwiched between the tungsten plates as the active medium. In Pb + Pb collisions, the ZDCs primarily measure “spectator” neutrons that do not interact hadronically when the incident nuclei collide.

Centrality in Pb+Pb collisions is determined by measuring the total transverse energy deposited in a liquid-argon forward calorimeter (FCal), which covers the pseudorapidity range $3.1 < |\eta| < 4.9$. The FCal is approximately ten interaction lengths deep, and consists of three modules: the first, with copper absorbers, is optimized for electromagnetic measurements, while the other two, with tungsten absorbers, are mainly sensitive to energy depositions associated with produced hadrons.

A two-level trigger system is used to select events of interest [27]. The first-level (L1) trigger is implemented in hardware and uses a subset of detector information to reduce the event rate to a design value of at most 100 kHz. This is followed by the software-based high-level trigger (HLT), which reduces the event rate to about 1–4 kHz. The L1 muon trigger requires coincidences between hits on different RPC or TGC planes, which are used as a seed for the HLT algorithms. The HLT uses dedicated algorithms to incorporate information from both the MS and the ID, achieving position and momentum resolution close to that provided by the offline muon reconstruction, as shown in Ref. [27].

An extensive software suite [28] is used in the reconstruction and analysis of real and simulated data, in detector operations, and in the trigger and data acquisition systems of the experiment. The offline event selection required that events pass in-time pileup cuts based on the ZDC energy.

III. DATA SELECTION AND SIMULATION SAMPLES

The results presented in this paper were obtained using pp data recorded in 2017 at a center-of-mass energy of 5.02 TeV

as well as Pb+Pb data collected in 2015 and 2018 at 5.02 TeV per nucleon-nucleon pair.

The integrated luminosity of the analyzed pp collision samples is 0.26 fb^{-1} . The pp events were collected using a dimuon trigger which requires at least two spatially separated muon candidates at L1, while both satisfy the criterion of $p_T^\mu > 4 \text{ GeV}$ in the HLT. For the Pb+Pb analysis, the integrated luminosity is 0.44 nb^{-1} for the 2015 data sample and 1.38 nb^{-1} for the 2018 data sample. Pb+Pb events were collected using triggers which require at least one muon with $p_T^\mu > 4 \text{ GeV}$ at both L1 and the HLT, and at least one additional muon satisfying $p_T^\mu > 4 \text{ GeV}$ in the HLT, without requiring matching to L1.

Muon pairs were required to fulfill the following criteria: at least one reconstructed muon matching the HLT’s dimuon trigger, and both muons matching the HLT without an L1 trigger requirement; both muons satisfy the *Medium* identification criteria (described in Ref. [29]) without any requirements on TRT hits; both muons are associated with the primary vertex reconstructed using all of the tracks in each event; the muon pair has a dimuon mass $7.7 < m_{\mu\mu} < 12.3 \text{ GeV}$, dimuon transverse momentum $|p_T^{\mu\mu}| < 30 \text{ GeV}$, and dimuon rapidity $|y^{\mu\mu}| < 1.5$; the selected muon pair is refitted to a common vertex, with the vertex fit quality satisfying $\chi^2 < 100$ and the significance of the transverse displacement of the refitted vertex relative to the primary vertex satisfying $|L_{xy}/\sigma(L_{xy})| < 3$, where $\sigma(L_{xy})$ is the primary-vertex resolution. The dimuon rapidity requirement was chosen to be $|y^{\mu\mu}| < 1.5$ because at more forward rapidities the Υ mass resolution starts to deteriorate quickly.

Monte Carlo (MC) simulation is used to study the $\Upsilon(nS)$ acceptance, the fit model used in Υ signal extraction, and the closure of muon reconstruction and identification corrections (due to residual biases associated with the yield correction procedure). The unpolarized prompt $\Upsilon(nS)$ in pp events was generated with the CTEQ6L1 [30] parton distribution function set in Pythia8 [31] with subsequent decay in muon pairs. Pythia8 implements prompt $\Upsilon(nS)$ production subprocesses using the nonrelativistic QCD Color Octet mechanism [32]. Prompt $\Upsilon(nS)$ production includes prompt production from the hard interactions, as well as the radiative feeddown from $\chi_b \rightarrow \Upsilon(nS)\gamma$ decays. The production of nonprompt J/ψ , used for determining per-muon corrections, was simulated in Pythia8 by forcing $b\bar{b}$ production and retaining only events consistent with J/ψ decays. The Pb+Pb MC sample was created by overlaying simulated Pythia8 pp events with recorded minimum-bias Pb+Pb events, so that the “data overlay” simulation samples contain the same level of underlying-event activity as is present in the Pb+Pb data. The response of the ATLAS detector was simulated [33] using GEANT4 [34]. The MC events are reconstructed with the same algorithms as used in data.

IV. ANALYSIS PROCEDURE

A. Centrality definition in Pb + Pb

The transverse energy measured in the forward calorimeter, ΣE_T^{FCal} , in minimum bias events, is used to estimate the

degree of overlap between the two colliding Pb nuclei. Each centrality class corresponds to a fixed percentile in the ΣE_T^{FCal} distribution of minimum-bias events using the procedure described in Ref. [21], where a table containing exact centrality bin definitions can be found. A Monte Carlo Glauber-based model [35] is used to calculate the mean number of participant nucleons, $\langle N_{\text{part}} \rangle$, and the mean nuclear overlap function, $\langle T_{AA} \rangle$, for each centrality class.

B. Corrections to raw invariant mass distributions

Before the dimuon invariant mass distributions are fit to extract Upsilon yields, each candidate dimuon pair is corrected with a weight that accounts for the $\Upsilon(nS)$ dimuon acceptance, trigger efficiency, and reconstruction efficiency.

The kinematic acceptance \mathcal{A} is defined as the probability that both muons from $\Upsilon \rightarrow \mu^+\mu^-$ decay pass the fiducial selection ($p_T^\mu > 4 \text{ GeV}$ and $|\eta^\mu| < 2.4$). The kinematic acceptance is calculated from a generator-level simulation separately for different $\Upsilon(nS)$ states as described in Ref. [36]. The acceptance correction also accounts for final-state radiation from one or both of the decay muons. In principle, the acceptance could depend on the spin alignment of the $\Upsilon(nS)$. In this analysis, $\Upsilon(nS)$ mesons are assumed to be produced unpolarized, following the previous measurements in pp collisions [37–39]. These measurements are consistent with no Υ polarization, but have large uncertainties. No extra systematic uncertainty due to Υ polarization is added in this paper.

The dimuon reconstruction efficiency, $\varepsilon_{\text{reco}}(\mu_1\mu_2)$, is determined as the product of two single-muon reconstruction efficiencies. The single-muon reconstruction efficiency is factorized into ID track reconstruction efficiency and MS reconstruction efficiency. For pp collisions, the values of the reconstruction efficiency are obtained from the $J/\psi \rightarrow \mu^+\mu^-$ Pythia8 simulation, and additional data-to-MC efficiency scale factors are derived using a $J/\psi \rightarrow \mu^+\mu^-$ tag-and-probe method [29] using pp data to account for residual differences between data and simulation. The same $J/\psi \rightarrow \mu^+\mu^-$ tag-and-probe method is employed to measure the muon reconstruction efficiency in Pb+Pb collisions. The ID reconstruction efficiency is obtained directly from Pb+Pb data, with a requirement on the transverse displacement of the J/ψ vertex to suppress potential biases from displaced muons. The MS reconstruction efficiency is obtained from the $J/\psi \rightarrow \mu^+\mu^-$ Pythia8 simulation overlaid with minimum-bias Pb+Pb data, and additional data-to-MC scale factors are determined in Pb+Pb data to account for the small difference between data and simulation. The ID reconstruction efficiency is found to be larger than 99% in both pp and Pb+Pb collisions, with a weak centrality dependence at low p_T^μ in the latter case. The MS reconstruction efficiency at $p_T^\mu = 4 \text{ GeV}$ is about 65% in the barrel region ($|\eta_\mu| < 1.05$) and 75% in the endcap region ($1.05 < |\eta_\mu| < 2.4$), and the MS efficiency increases with p_T^μ and saturates at 95% around $p_T^\mu = 7 \text{ GeV}$ in both the barrel and endcap regions. Due to the absorption of most hadronic activity in the ATLAS calorimeters, the MS reconstruction efficiency has no centrality dependence. For a given muon pair, the dimuon trigger efficiency in pp collisions

is factorized as the product of two single-muon efficiencies. The dimuon trigger efficiency in Pb + Pb collisions is the combined efficiency of either of the two muons matching the HLT trigger with the other one matching the HLT trigger without L1 trigger requirement.

The single-muon trigger efficiency is determined in data and simulation using a $J/\psi \rightarrow \mu^+\mu^-$ tag-and-probe method similar to that used for the muon reconstruction efficiency. Two different muon-trigger logic schemes are used in this analysis: (1) a full-chain muon trigger, which requires the formation of an L1 muon candidate that is subsequently confirmed in the HLT, and (2) a full-scan muon trigger, which is only performed in the HLT via a muon candidate search of the full MS system without any requirement at L1. The values of the full-chain muon trigger efficiency are determined from MC simulation, with data-to-MC scale factors determined from the pp data to take into account the difference between data and simulation. The same values are used for pp and Pb+Pb collisions, except that an additional centrality-dependent correction is applied to Pb+Pb data. The centrality-dependent correction is determined as the ratio of the trigger efficiency measured in Pb+Pb collisions as a function of centrality to the trigger efficiency in pp data. The full-chain muon trigger efficiency plateau value is found to be 70% in the barrel and 90% in the endcaps. The centrality-dependent correction factor is about 90% (100%) for the 0–10% (60–80%) centrality range. The full-scan muon trigger is only used in Pb+Pb collisions and its efficiency is determined directly from Pb+Pb data, using the tag-and-probe method. The full-scan trigger plateau is found to be 90% in both the barrel and endcap regions. The dimuon trigger efficiency in pp collisions is factorized as the product of two full-chain muon trigger efficiencies, and in Pb+Pb collisions the factorization form consisting of full-chain and full-scan muon trigger efficiencies, as detailed in Ref. [21], is used.

C. Upsilon signal extraction

Upsilon states are reconstructed in the $\mu^+\mu^-$ decay channel and their yields are determined via unbinned maximum-likelihood fits to the weighted dimuon invariant mass distributions, following the same procedure for both pp and Pb+Pb data. Each of the three $\Upsilon(nS)$ state signal shapes is described by a sum of Crystal Ball (CB) [40] and Gaussian functions.

The probability distribution function for the fit is defined as a normalized sum of three Υ signal components and a background component as

$$\text{pdf}(m_{\mu\mu}) = N_{\Upsilon(1S)}f_{\Upsilon(1S)}(m_{\mu\mu}) + N_{\Upsilon(2S)}f_{\Upsilon(2S)}(m_{\mu\mu}) \\ + N_{\Upsilon(3S)}f_{\Upsilon(3S)}(m_{\mu\mu}) + N_{\text{bkg}}f_{\text{bkg}}(m_{\mu\mu}),$$

where $f_{\Upsilon(nS)}(m_{\mu\mu}) = \omega F_G(m_{\mu\mu}; M_{nS}, \sigma_{nS}) + (1 - \omega)F_{CB}(m_{\mu\mu}; M_{nS}, 1.7\sigma_{nS}, \alpha, n)$; $N_{\Upsilon(nS)}$ and N_{bkg} are the Upsilon and background yields, respectively; and F_G and F_{CB} are Gaussian and Crystal Ball functions, respectively, with ω representing relative weight of the Gaussian function. The quantities M_{nS} and σ_{nS} are the Gaussian function's mean and width for

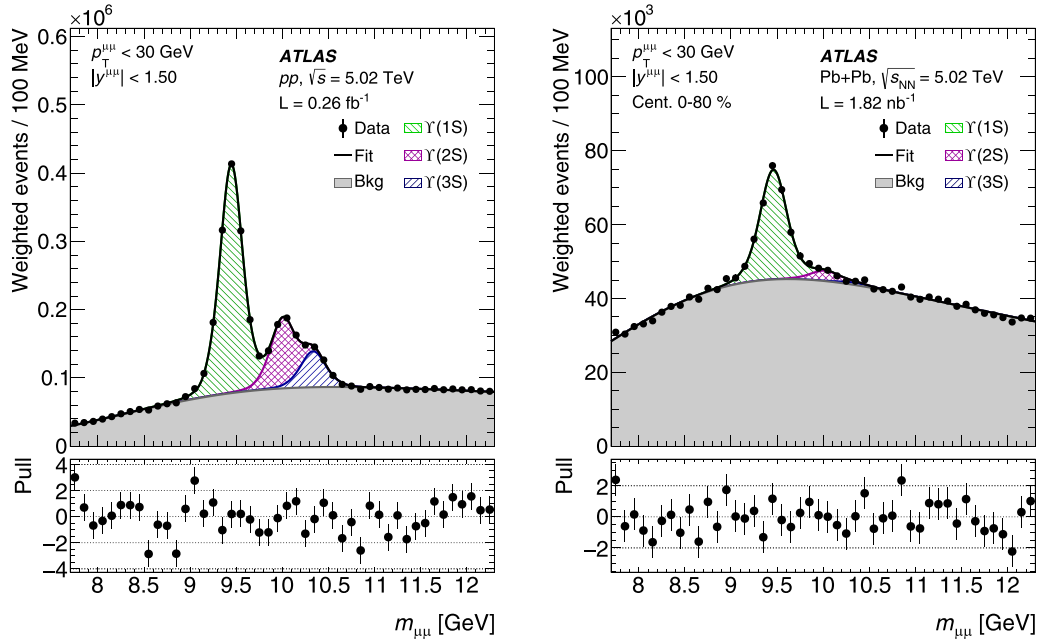


FIG. 1. Dimuon invariant mass distributions with the fit results for pp (left) and Pb+Pb (right) collisions at 5.02 TeV. The various curves are explained in the legend. Pull distributions are shown in the lower panels. For this selection, χ^2/NDF is 2.7 for pp and 1.3 for Pb + Pb.

each Upsilon state, and α and n are F_{CB} tail parameters. The line-shape parameters are assumed to be the same for all three Υ states since it is mostly determined by detector effects. The background shape, $f_{\text{bkg}}(m_{\mu\mu})$, is represented by a second-order polynomial at high $p_{\text{T}}^{\mu\mu}$ ($p_{\text{T}}^{\mu\mu} > 6$ GeV) and as a product of an error function and an exponential function at low $p_{\text{T}}^{\mu\mu}$.

The determination of the yield corrected for acceptance and efficiencies, $N_{\Upsilon(n\text{S})}^{\text{corr}}$, proceeds in several steps. First, a resonance-dependent weight, $w_{\text{total}}[\Upsilon(n\text{S})]$, is determined for each selected dimuon candidate as

$$w_{\text{total}}[\Upsilon(n\text{S})] = \frac{1}{\mathcal{A}[\Upsilon(n\text{S})]\varepsilon_{\text{reco}}(\mu_1\mu_2)\varepsilon_{\text{trig}}(\mu_1\mu_2)\varepsilon_{\text{pvAsso}}(\mu_1\mu_2)},$$

where $\mathcal{A}[\Upsilon(n\text{S})]$ is the acceptance for $\Upsilon(n\text{S}) \rightarrow \mu^+\mu^-$ decay, $\varepsilon_{\text{reco}}$ is the muon reconstruction efficiency, $\varepsilon_{\text{trig}}$ is the trigger efficiency, and $\varepsilon_{\text{pvAsso}}$ is the efficiency related to the primary-vertex association. Next, an unbinned maximum-likelihood fit to the weighted dimuon invariant mass distribution ($m_{\mu\mu}$) is performed to extract the $\Upsilon(n\text{S})$ yields. Three fits with an acceptance value corresponding to each state are performed to extract the yields for the three Υ states.

The mean and Gaussian width of the $\Upsilon(1\text{S})$ signal, $M_{1\text{S}}$ and $\sigma_{1\text{S}}$, are left unconstrained in each $p_{\text{T}}^{\mu\mu}$, $|y^{\mu\mu}|$, and centrality range, while the means and widths of $\Upsilon(2\text{S})$ and $\Upsilon(3\text{S})$ in the same range are fixed to $\Upsilon(1\text{S})$ parameters scaled by the respective Particle Data Group [41] mass ratios. The widths of the CB functions are set by scaling the corresponding Gaussian widths by a constant factor, 1.7, which was determined in a previous analysis [42] and validated with MC studies. The relative weight of the Gaussian and CB functions, ω , is not constrained, and has the same value for all three Upsilon

states. For the pp collision analysis, the CB function parameter α , which defines the point at which the low-mass tail transitions from a Gaussian shape to a power-law shape, was fixed to the value obtained from $\Upsilon(1\text{S})$ MC samples, while n , which describes the shape of the tail, was a free parameter. For Pb + Pb collisions, both α and n were fixed to the values from the fit for pp collisions, for each kinematic selection. The nominal signal fit model described above was validated by fitting the signal MC samples in various $p_{\text{T}}^{\mu\mu}$, $|y^{\mu\mu}|$, and centrality intervals.

The background functional form varies with dimuon $p_{\text{T}}^{\mu\mu}$. For $p_{\text{T}}^{\mu\mu} > 6$ GeV the background is parametrized as a second-order polynomial. However, for lower $p_{\text{T}}^{\mu\mu}$ ($p_{\text{T}}^{\mu\mu} < 6$ GeV), and for the integrated over $p_{\text{T}}^{\mu\mu}$ fits, in order to describe the turn-on behavior of the dimuon acceptance caused by the single-muon transverse momentum requirement, an error function multiplied by an exponential function is used. The background model parameters are initialized using a background-enriched sample, which consists of events with same-sign muon pairs, as well as a control sample consisting primarily of muons from b-hadron decays. The control sample is produced by requiring at least one of the two muons to satisfy $|d_0|/\sigma_{d_0} > 2$ or $|z_0 \sin(\theta)| > 0.2$ mm, where d_0 and z_0 are the distances of closest approach of the muon to the primary vertex in the plane perpendicular to the beam and in the beam direction, respectively. After using the background distributions to determine the relevant parametrizations, the full model including signal and background contributions is used to fit the data, with the slope of the exponential function allowed to float.

Figure 1 shows an example of the fit to the dimuon mass plots for pp (left) and 0–80% centrality Pb+Pb (right) collisions for the inclusive $p_{\text{T}}^{\mu\mu}$ and $|y^{\mu\mu}|$ selection. The lower panels show the pull distribution, which represents the

TABLE I. Summary of the sources of systematic uncertainty.

| Collision type | Sources | $\Upsilon(1S)$ (%) | $\Upsilon(nS)$ (%) | $\Upsilon(nS)/\Upsilon(1S)$ (%) |
|----------------------|----------------------------|--------------------|--------------------|---------------------------------|
| <i>pp</i> collisions | Luminosity | 1.6 | 1.6 | |
| | Acceptance | 0.3–9.3 | 0.2–4.1 | |
| | Efficiency | 2.7–7.0 | 2.8–4.0 | 3.0–7.1 |
| | Signal extraction | 3.1–10.2 | 4.3–11.9 | 4.5–12.2 |
| | Bin migration | <1 | <1 | |
| | Primary-vertex association | 2.0 | 2.0 | |
| Pb+Pb collisions | $\langle T_{AA} \rangle$ | 0.8–8.2 | 0.8–8.2 | |
| | Acceptance | 0.3–9.3 | 0.2–4.1 | |
| | Efficiency | 4.0–15.0 | 3.9–25.3 | 4.4–28.8 |
| | Signal extraction | 3.8–16.3 | 14.6–28.7 | 16.6–31.5 |
| | Bin migration | <2 | <2 | |
| | Primary-vertex association | 3.4 | 3.4 | |

distance between data points and fit function normalized by the data points' statistical uncertainty: $(\text{Data} - \text{Fit})/\sigma(\text{Data})$. The goodness of the fit is assessed by calculating the reduced chisquare, χ^2/NDF , summing the squared deviations of the data points from the fit (weighted by the inverse errors) and then dividing by the number of degrees of freedom (NDF) in the fit. Typically, χ^2/NDF for the fits varies from ≈ 2.5 to ≈ 1 for *pp* and from ≈ 2 to ≈ 1 for Pb + Pb, indicating that the data and model agree within statistical uncertainties. The extracted values of χ^2/NDF decrease with $p_T^{\mu\mu}$, indicating that the fit quality improves with $p_T^{\mu\mu}$. Some relatively large χ^2/NDF values are also found and can be explained by deviations of the functions used for background description from the actual background at the edges of the fit range.

D. Systematic uncertainties

The main sources of point-by-point uncorrelated systematic uncertainties pertain to the corrections for muon reconstruction and trigger efficiencies, and the yield extraction. For the lowest $p_T^{\mu\mu}$ range, the final-state radiation correction is also a significant contribution. Other subdominant sources of systematic uncertainty considered in this paper are the primary-vertex association uncertainty and bin migration due to momentum resolution. Finally, the Upsilon states are assumed to be unpolarized and no extra systematic uncertainty is assigned to cover this assumption.

The systematic uncertainty in the MS reconstruction efficiency is dominated by the uncertainty in the data-to-MC scale-factor determination. The scale-factor uncertainty is evaluated following Ref. [29] by changing the tag-muon selection criteria and varying the line shapes in the efficiency extraction fit procedure in the data. The uncertainty related to the ID reconstruction efficiency, which is close to 1, is estimated by comparing the results while varying this efficiency in both up and down directions by one standard deviation.

The systematic uncertainty in the muon trigger efficiency is also dominated by the tag-and-probe efficiency determination procedure. For Pb+Pb collisions, an additional systematic uncertainty associated with the centrality-dependent correction is included. This uncertainty is evaluated by comparing the centrality-dependence-corrected Pb+Pb

efficiency with the *pp* efficiency as a function of p_T^{μ} . Individual variations described above are added in quadrature to form the total systematic uncertainty of the efficiency corrections.

The sensitivity of the signal extraction to the choice of a particular fit model is evaluated by varying the line shape of each fit component. The maximum variation between the recalculated values and the central value is used to estimate their uncertainty. Eight variations are considered, and these can be categorized into three groups: signal resolution (width of the peak), shape of the final-state radiation tail, and background shape. The final uncertainty from the fit model is obtained by calculating the difference between the maximum and the minimum yield from the eight line-shape variations and dividing by $\sqrt{12}$, assuming a flat distribution.

The uncertainty in the Υ acceptance due to the final-state radiation correction was calculated by comparing the result of a fully simulated acceptance calculation with that obtained using an MC sample designed for a high-precision determination of the acceptance. The signal Monte Carlo samples were processed with a fast simulation [33] which relies on a parametrization of the calorimeter response [43]. This uncertainty is only important for the lowest $p_T^{\mu\mu}$ range.

The global uncertainty of the integrated luminosity for the 2017 *pp* data is 1.6%, derived using methods described in Ref. [44]. Primary-vertex association uncertainty, which results mostly from small discrepancies between data and MC, was studied by varying the primary-vertex association requirements. Since the primary-vertex association affects all Upsilon state yields in the same way, it is treated as a global uncertainty together with those of the *pp* luminosity and T_{AA} . The combined systematic uncertainty for the luminosity and primary-vertex association in *pp* data is 2.6%. For Pb+Pb collisions, the global systematic uncertainty of $\langle T_{AA} \rangle$ is estimated by varying the Glauber model parameters as detailed in Ref. [45]. The combined systematic uncertainty for $\langle T_{AA} \rangle$ and primary-vertex association in Pb+Pb collisions is 3.7%.

Systematic uncertainties in *pp* and Pb + Pb collisions are summarized in Table I. While some systematic uncertainties for R_{AA} values and excited-state to ground-state double ratios are correlated (e.g., the acceptance) and cancel out in the

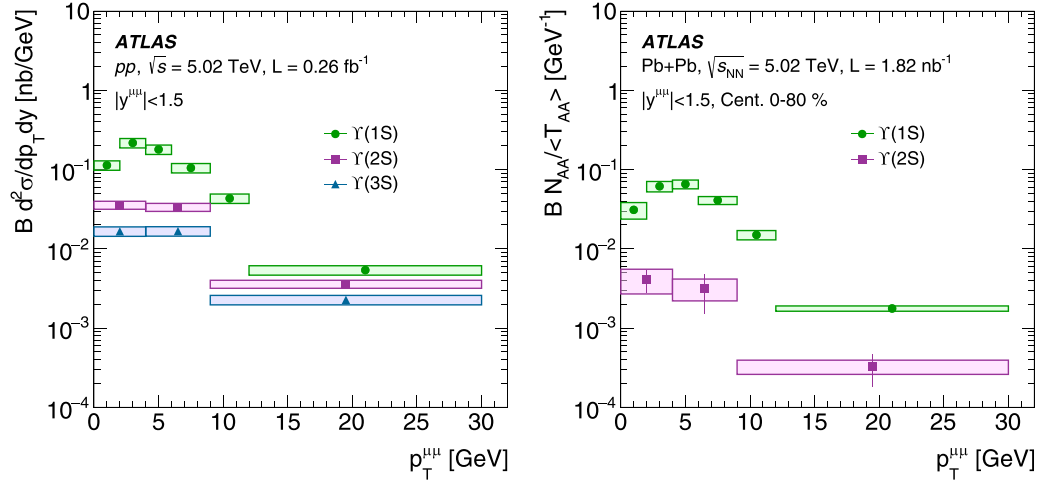


FIG. 2. Production cross sections of $\Upsilon(1S)$, $\Upsilon(2S)$, and $\Upsilon(3S)$ mesons as a function of $p_T^{\mu\mu}$ in pp collisions (left) and per-event yields in $Pb+Pb$ collisions (right) at 5.02 TeV. Error bars indicate the statistical uncertainties and boxes represent the systematic uncertainties. Not shown are the correlated systematic uncertainties of 2.6% for luminosity and primary-vertex association in pp and 3.7% for $\langle T_{AA} \rangle$ and primary-vertex association in $Pb+Pb$ collisions.

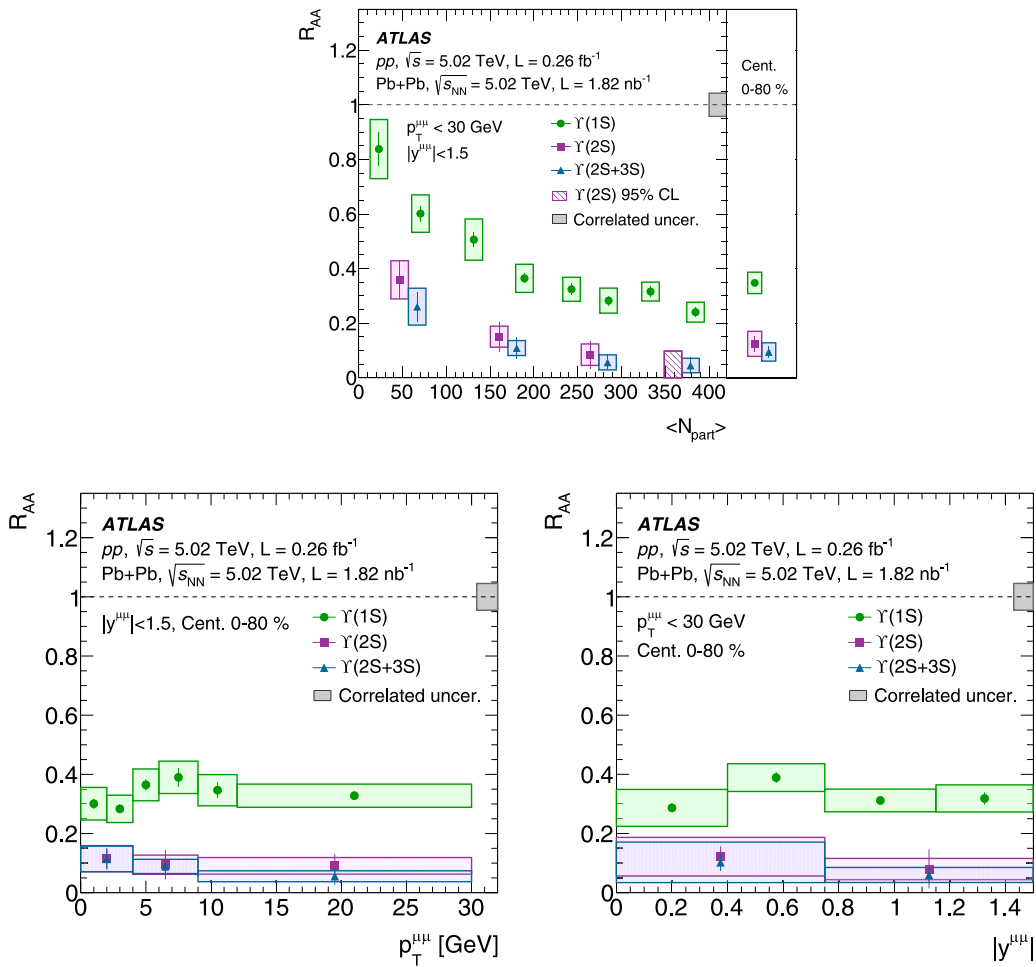


FIG. 3. The nuclear modification factor R_{AA} of $\Upsilon(1S)$, $\Upsilon(2S)$, and $\Upsilon(2S + 3S)$ as functions of centrality (top), $p_T^{\mu\mu}$ (bottom left), and $|y^{\mu\mu}|$ (bottom right) at 5.02 TeV. Error bars indicate the statistical uncertainties and boxes represent the systematic uncertainties. The gray boxes around $R_{AA} = 1$ correspond to the global systematic uncertainty. The right panel of the top plot shows the R_{AA} results integrated over centrality.

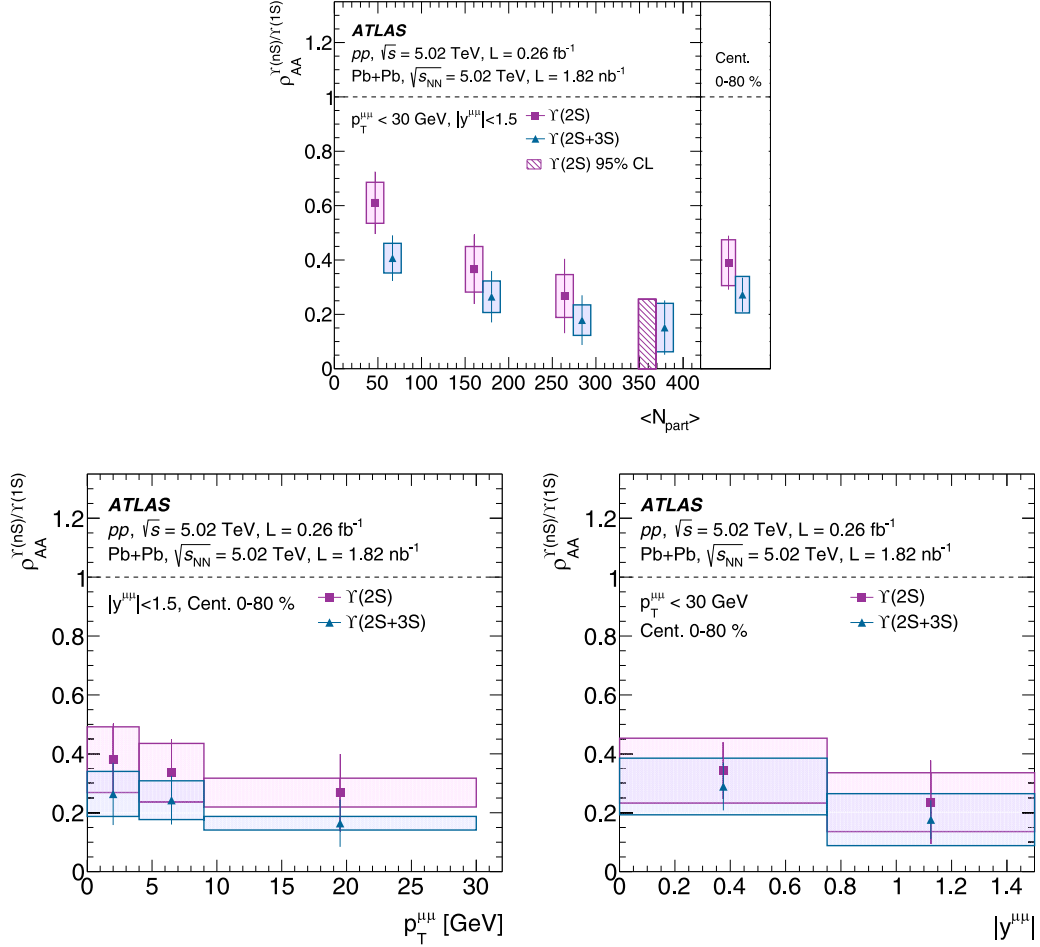


FIG. 4. The double ratio $\rho_{AA}^{\Upsilon(nS)/\Upsilon(1S)}$ for $\Upsilon(2S)$ and $\Upsilon(2S+3S)$ as functions of centrality (top), $p_T^{\mu\mu}$ (bottom left), and $|y^{\mu\mu}|$ (bottom right) at 5.02 TeV per nucleon-nucleon pair. Error bars indicate the statistical uncertainties and boxes represent the systematic uncertainties. The right panel of the top plot shows the results integrated over centrality.

ratios, most of the systematic uncertainties are not completely correlated and are estimated by directly studying their effects on the ratios.

V. RESULTS

A. Differential cross section

Differential $\Upsilon(nS)$ production cross sections in pp collisions are measured according to the relation

$$\frac{d^2\sigma_{\Upsilon(nS)}}{dp_T^{\mu\mu} dy^{\mu\mu}} \mathcal{B}(\Upsilon(nS) \rightarrow \mu^+ \mu^-) = \frac{N_{\Upsilon(nS)}^{\text{corr}}}{\Delta p_T^{\mu\mu} \Delta y^{\mu\mu} \int \mathcal{L} dt},$$

where $\mathcal{B}[\Upsilon(nS) \rightarrow \mu^+ \mu^-]$ is the dimuon decay branching fraction, $N_{\Upsilon(nS)}^{\text{corr}}$ is the $\Upsilon(nS)$ yield corrected for acceptance and efficiencies, $\Delta p_T^{\mu\mu}$ and $\Delta y^{\mu\mu}$ are the bin widths in $p_T^{\mu\mu}$ and $y^{\mu\mu}$, and $\int \mathcal{L} dt$ is the integrated luminosity.

The $\Upsilon(nS)$ differential cross sections in pp collisions at 5.02 TeV, multiplied by the respective dimuon branching fractions, are shown as a function of $p_T^{\mu\mu}$ in the left panel of Fig. 2.

The per-event yields of $\Upsilon(nS)$ states in Pb+Pb collisions are defined by

$$N_{AA} = \frac{N_{\Upsilon(nS)}^{\text{corr}}}{\Delta p_T^{\mu\mu} \Delta y^{\mu\mu} N_{\text{evt}}},$$

where N_{evt} is the total number of minimum-bias Pb+Pb collisions in each centrality class. In particular, this number is 1.02×10^9 for the 0–10% centrality interval. Per-event Upsilon yields in Pb+Pb collisions divided by $\langle T_{AA} \rangle$ are shown in the right panel of Fig. 2. The results for $\Upsilon(3S)$ mesons are not shown because their peaks are not statistically significant in Pb+Pb collisions.

B. Nuclear modification factor

The modifications of bottomonium production yields in Pb+Pb collisions relative to the pp system are quantified by the nuclear modification factor R_{AA} , which can be defined for each centrality interval as

$$R_{AA} = \frac{N_{AA}}{\langle T_{AA} \rangle \sigma^{pp}},$$

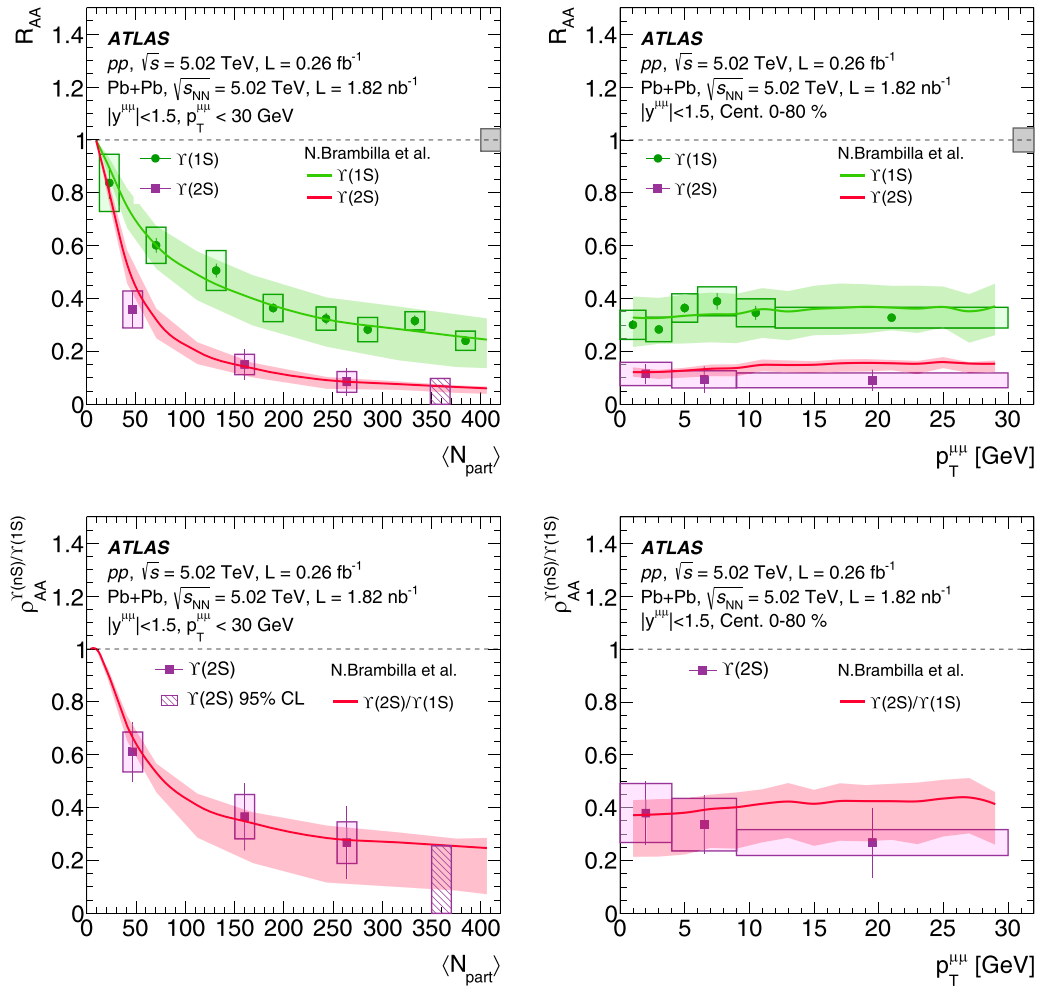


FIG. 5. The nuclear modification factor R_{AA} of $\Upsilon(1S)$ and $\Upsilon(2S)$ (top row) and the double ratio $\rho_{AA}^{\Upsilon(nS)/\Upsilon(1S)}$ for $\Upsilon(1S)$ and $\Upsilon(2S)$ (bottom row) as functions of centrality (left column) and $p_T^{\mu\mu}$ (right column) at 5.02 TeV per nucleon-nucleon pair compared to a calculation by Brambilla *et al.* [46] (solid curves). Color bands represent model uncertainties due to variation of the model parameters.

where N_{AA} is the observed per-event yield of bottomonium states in Pb+Pb collisions, and σ^{pp} is the bottomonium production cross section in pp collisions at the same collision energy.

Figure 3 shows the R_{AA} values of $\Upsilon(nS)$ as functions of $\langle N_{part} \rangle$ (top), dimuon $p_T^{\mu\mu}$ (bottom left), and $|y^{\mu\mu}|$ (bottom right). The centrality-integrated results are also shown in the right panel of the top plot. In addition to the results for $\Upsilon(1S)$ and $\Upsilon(2S)$, only the combined result for the two excited states, $\Upsilon(2S + 3S)$, is presented because the $\Upsilon(3S)$ peak is not statistically significant in the Pb+Pb data. The $\Upsilon(nS)$ states are observed to be suppressed over the whole kinematic range investigated, and the R_{AA} values of $\Upsilon(2S)$ and $\Upsilon(2S + 3S)$ are always lower than those of $\Upsilon(1S)$. The R_{AA} value decreases with $\langle N_{part} \rangle$ for all three states. No strong $p_T^{\mu\mu}$ or $|y^{\mu\mu}|$ dependence is observed. When no statistically significant nonzero yield was extracted for a particular kinematic selection, the 95% confidence level upper limit was calculated.

C. Excited-state to ground-state double ratios

The suppression of different Upsilon states can be compared by constructing an excited-state to ground-state double

ratio of nuclear modification factors. The advantage of measuring the double ratios is that the acceptance and efficiency corrections partially cancel out, and the overall systematic uncertainty is reduced. Although defined in terms of the individual nuclear suppression factors, the double ratio can be understood as being defined as the ratio of the yields of excited states $\Upsilon(2S)$ and $\Upsilon(3S)$ or of the combined yield of the two excited states [$\Upsilon(2S + 3S)$] to the yield of the ground state $\Upsilon(1S)$ in Pb+Pb collisions, divided by the same ratio in pp collisions:

$$\rho_{AA}^{\Upsilon(nS)/\Upsilon(1S)} = R_{AA}[\Upsilon(nS)]/R_{AA}[\Upsilon(1S)].$$

Figure 4 shows the $\rho_{AA}^{\Upsilon(nS)/\Upsilon(1S)}$ for $\Upsilon(2S)$ and $\Upsilon(2S + 3S)$ as functions of N_{part} (top), $p_T^{\mu\mu}$ (bottom left), and $|y^{\mu\mu}|$ (bottom right). The centrality-integrated results are also shown in the right panel of the top plot. The $\rho_{AA}^{\Upsilon(nS)/\Upsilon(1S)}$ values for $\Upsilon(2S)$ and $\Upsilon(2S + 3S)$ are always less than 1, indicating the excited states are more suppressed than the ground state. The centrality-dependent $\rho_{AA}^{\Upsilon(nS)/\Upsilon(1S)}$ shows a slightly decreasing trend toward more central collisions, but no $p_T^{\mu\mu}$ or $|y^{\mu\mu}|$ dependence is observed.

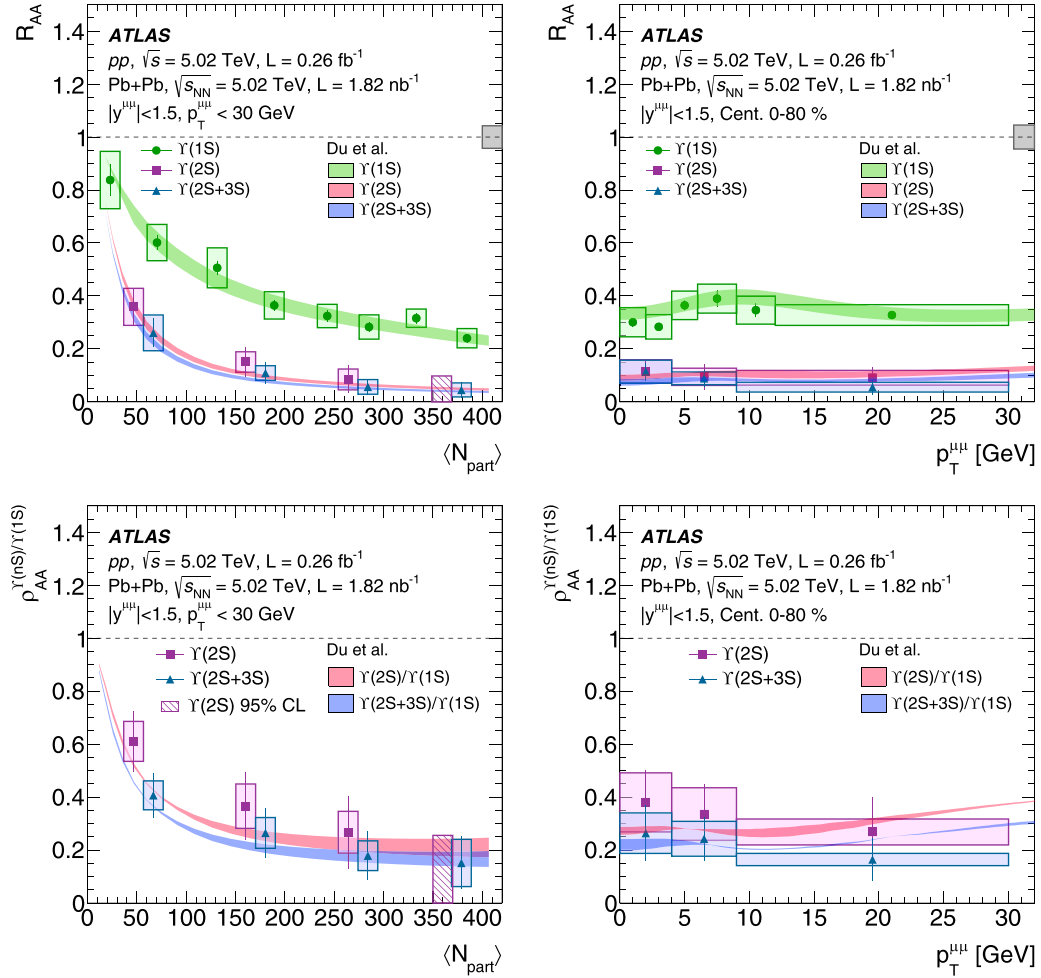


FIG. 6. The nuclear modification factor R_{AA} of $\Upsilon(1S)$ and $\Upsilon(2S)$ (top row) and the double ratio $\rho_{AA}^{\Upsilon(ns)/\Upsilon(1s)}$ for $\Upsilon(2S)$ (bottom row) as functions of centrality (left) and $p_T^{\mu\mu}$ (right) at 5.02 TeV per nucleon-nucleon pair compared to a calculation by Du *et al.* [47]. The bands represent 95% confidence level (CL) limits.

These results are consistent with previous measurements of Upsilon suppression at LHC energies by the CMS [11] and ALICE [13] experiments.

D. Theory comparisons and discussion

Figure 5 shows the R_{AA} of $\Upsilon(1S)$ and $\Upsilon(2S)$ and the double ratio $\rho_{AA}^{\Upsilon(2S)/\Upsilon(1S)}$ compared with a calculation by Brambilla *et al.* in Ref. [46]. This model uses potential Non-relativistic quantum chromodynamics and the formalism of open quantum systems to numerically solve the Lindblad equation using a stochastic unraveling called the quantum trajectories algorithm. Heavy-quark interactions with the strongly coupled medium are encoded in the two nonperturbative transport coefficients: the heavy-quark momentum diffusion coefficient and its dispersive counterpart. The authors of Ref. [46] have run variations of these parameters within reasonable ranges.

Figure 6 shows the R_{AA} of $\Upsilon(1S)$, $\Upsilon(2S)$, and $\Upsilon(2S + 3S)$, and the double ratio $\rho_{AA}^{\Upsilon(ns)/\Upsilon(1s)}$ for $\Upsilon(2S)$ and $\Upsilon(2S + 3S)$ compared to a calculation by Du *et al.* in Ref. [47]. This model uses a kinetic-rate equation approach including regeneration

and has four dimensionless parameters which characterize the temperature dependence of the pertinent screening masses. These parameters are extracted through the fits to the data already available at RHIC and LHC. The band corresponding to the 95% confidence interval is shown in the figure.

Figure 7 shows the R_{AA} of $\Upsilon(1S)$, $\Upsilon(2S)$, and $\Upsilon(2S + 3S)$, as well as the double ratio $\rho_{AA}^{\Upsilon(ns)/\Upsilon(1s)}$ for $\Upsilon(1S)$ and $\Upsilon(2S)$, compared to a calculation by Yao *et al.* in Ref. [8]. This model uses a framework with coupled transport equations for open heavy-flavor and quarkonium states in order to describe their transport inside the quark-gluon plasma, including regeneration. Cold nuclear matter effects are included by using nuclear parton distribution functions for the initial primordial heavy-flavor production. A calibrated (2 + 1)-dimensional viscous hydrodynamic model is used to describe the bulk QCD medium. The model depends on the choice of nucleus parton distribution function and two coupling constant parameters, α_s and α_s^{pot} , which are varied by $\pm 10\%$ from their nominal values.

All three models are in agreement with the data within experimental and theoretical uncertainties. It is notable that all

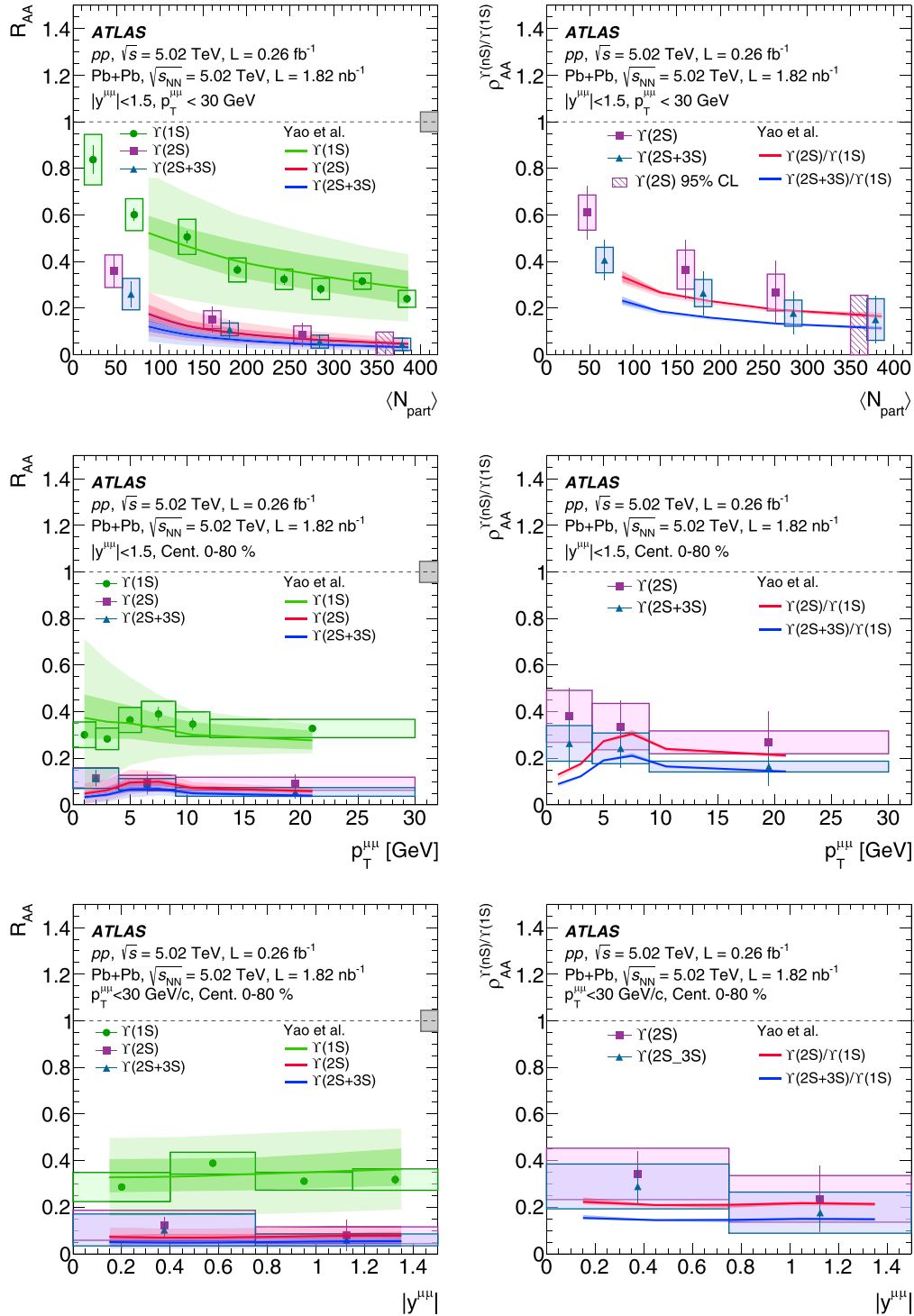


FIG. 7. The nuclear modification factor R_{AA} of $\Upsilon(1S)$, $\Upsilon(2S)$, and $\Upsilon(2S + 3S)$ (left column) and the double ratio $\rho_{AA}^{\Upsilon(ns)/\Upsilon(1S)}$ for $\Upsilon(2S)$ and $\Upsilon(2S + 3S)$ (right column) as functions of centrality (top row), $p_T^{\mu\mu}$ (center row), and rapidity (bottom row) at 5.02 TeV per nucleon-nucleon pair compared to a calculation by Yao *et al.* [8] (solid curves). Dark color bands show theory uncertainty due to the nucleus parton distribution function choice. Light color bands show model uncertainties due to varying the calculation parameters by $\pm 10\%$.

three theoretical results were calculated after the publication of a CMS measurement of Υ suppression in Ref. [11] at the same beam energy.

Figure 8 shows the ATLAS results presented in this paper compared with CMS published values [12] for the $\Upsilon(1S)$

(left) and $\Upsilon(2S)$ (right) states. These measured nuclear modification factors, as well as the double ratios, are consistent between ATLAS and CMS within uncertainties. The kinematic selections are similar, though ATLAS uses a narrow rapidity window $|y| < 1.5$ compared with $|y| < 2.4$ in CMS.

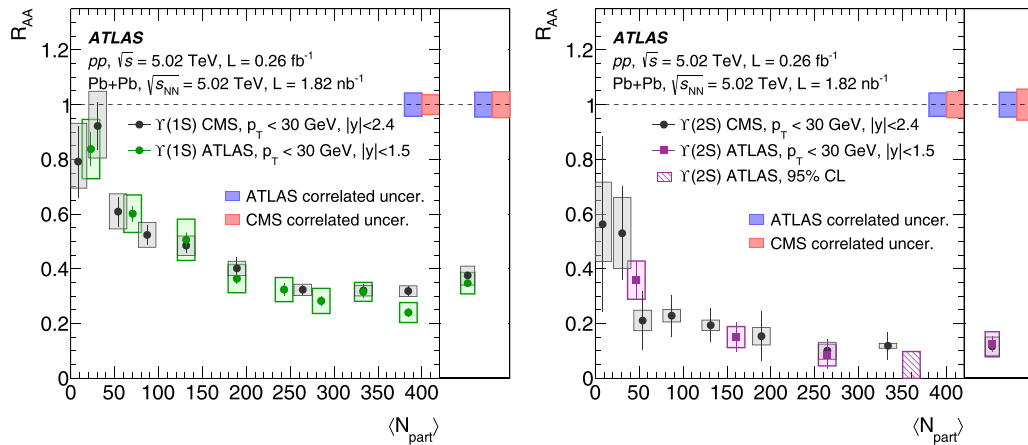


FIG. 8. The nuclear modification factor R_{AA} of $\Upsilon(1S)$ (left) and $\Upsilon(2S)$ (right) compared to the previous CMS measurement [12].

Published results by the ALICE Collaboration [13,14] are at more forward rapidities, and thus no direct comparison is made. The sequential melting of Upsilon states is thus confirmed by the present measurement. Suppression of the $\Upsilon(1S)$ observed at the level of approximately 0.25–0.30 in central Pb + Pb collisions indicates suppression of the directly produced $\Upsilon(1S)$ and not just suppression of higher states feeding down to the $\Upsilon(1S)$, thus providing important information on the highest temperatures achieved in the QGP.

More recently, CMS presented a measurement which includes the first observation of the $\Upsilon(3S)$ in Pb + Pb collisions at the LHC [48]. The $\Upsilon(3S)$ is even more suppressed than the $\Upsilon(1S)$ and $\Upsilon(2S)$, further quantifying the sequential melting of quarkonium states in QGP. The combined nuclear modification factor for the two excited states $\Upsilon(2S + 3S)$ presented in this paper is consistent with the $\Upsilon(3S)$ CMS measurement.

Reference [49] quotes dissociation temperatures in the case of an isotropic QGP of $\langle 192, 228, \text{ and } 593 \text{ MeV}$ for the $\Upsilon(3S)$, $\Upsilon(2S)$, and $\Upsilon(1S)$ states, respectively. It is notable that the $\Upsilon(1S)$ has a substantial decay feeddown fraction from $\Upsilon(2S)$, $\Upsilon(3S)$, $\chi_b(1S)$, and $\chi_b(2S)$ states, and that only about half of $\Upsilon(1S)$ are directly produced. Thus, the suppression at the level of approximately 0.25–0.30 for the $\Upsilon(1S)$ observed in central Pb + Pb collisions indicates at least some suppression of the directly produced $\Upsilon(1S)$, which has important implications regarding the temperatures achieved in the QGP.

VI. CONCLUSIONS

This paper presents a measurement of $\Upsilon(nS)$ yields in pp and Pb+Pb data at 5.02 TeV per nucleon-nucleon collision. The measurement uses data from pp collisions collected in 2017 with a total integrated luminosity of 0.26 fb^{-1} and Pb+Pb collisions collected in 2015 and 2018 with total integrated luminosities of 0.44 and 1.38 nb^{-1} , respectively, recorded by the ATLAS experiment at the LHC. The pp and Pb+Pb measurements are used to obtain the nuclear modification factor for $\Upsilon(1S)$, $\Upsilon(2S)$, and $\Upsilon(2S + 3S)$, as well as excited-state to ground-state double ratios of R_{AA} for $\Upsilon(2S)$ and $\Upsilon(2S + 3S)$ as functions of transverse momentum,

rapidity, and centrality. Both the $\Upsilon(1S)$ and $\Upsilon(2S)$ yields are suppressed with increasing centrality in Pb+Pb compared to those in pp collisions, and the excited states are shown to be more strongly suppressed than the ground state, resulting in double ratios smaller than 1. The R_{AA} value for $\Upsilon(2S + 3S)$ appears to be systematically lower than that for $\Upsilon(2S)$, and so are the corresponding double ratios, which indicates that the $\Upsilon(3S)$ state is suppressed more than $\Upsilon(2S)$.

The measured nuclear modification factors and double ratios are found to be consistent with the previous CMS measurement [12] at similar kinematical conditions.

All theoretical calculations considered in this paper describe the data well and incorporate deconfinement as a key ingredient in the suppression of the Upsilon yields. Further discrimination between the different implementations of these deconfinement effects requires additional precision data from upcoming runs at RHIC and the LHC.

ACKNOWLEDGMENTS

We thank CERN for the very successful operation of the LHC, as well as the support staff from our institutions without whom ATLAS could not be operated efficiently. We acknowledge the support of ANPCyT, Argentina; YerPhI, Armenia; ARC, Australia; BMWFW and FWF, Austria; ANAS, Azerbaijan; CNPq and FAPESP, Brazil; NSERC, NRC and CFI, Canada; CERN; ANID, Chile; CAS, MOST and NSFC, China; Minciencias, Colombia; MEYS CR, Czech Republic; DNRf and DNSRC, Denmark; IN2P3-CNRS and CEA-DRF/IRFU, France; SRNSFG, Georgia; BMBF, HGF and MPG, Germany; GSRI, Greece; RGC and Hong Kong SAR, China; ISF and Benozziyo Center, Israel; INFN, Italy; MEXT and JSPS, Japan; CNRST, Morocco; NWO, Netherlands; RCN, Norway; MEiN, Poland; FCT, Portugal; MNE/IFA, Romania; MESTD, Serbia; MSSR, Slovakia; ARRS and MIZŠ, Slovenia; DSI/NRF, South Africa; MICINN, Spain; SRC and Wallenberg Foundation, Sweden; SERI, SNSF and Cantons of Bern and Geneva, Switzerland; MOST, Taiwan; TENMAK, Türkiye; STFC, United Kingdom; DOE and NSF, United States of America. In addition, individual groups and members have received support from BCKDF, CANARIE,

Compute Canada and CRC, Canada; PRIMUS 21/SCI/017 and UNCE SCI/013, Czech Republic; COST, ERC, ERDF, Horizon 2020 and Marie Skłodowska-Curie Actions, European Union; Investissements d'Avenir Labex, Investissements d'Avenir Idex and ANR, France; DFG and AvH Foundation, Germany; Herakleitos, Thales and Aristeia programmes co-financed by EU-ESF and the Greek NSRF, Greece; BSF-NSF and MINERVA, Israel; Norwegian Financial Mechanism 2014-2021, Norway; NCN and NAWA, Poland; La Caixa Banking Foundation, CERCA Programme Generalitat de Catalunya and PROMETEO and GenT Programmes General-

itat Valenciana, Spain; Göran Gustafssons Stiftelse, Sweden; The Royal Society and Leverhulme Trust, United Kingdom. The crucial computing support from all WLCG partners is acknowledged gratefully, in particular from CERN; the ATLAS Tier-1 facilities at TRIUMF (Canada), NDGF (Denmark, Norway, Sweden), CC-IN2P3 (France), KIT/GridKA (Germany), INFN-CNAF (Italy), NL-T1 (Netherlands), PIC (Spain), ASGC (Taiwan), RAL (UK), and BNL (USA); the Tier-2 facilities worldwide; and large non-WLCG resource providers. Major contributors of computing resources are listed in Ref. [50].

- [1] T. Matsui and H. Satz, J/ψ suppression by quark-gluon plasma formation, *Phys. Lett. B* **178**, 416 (1986).
- [2] F. Karsch, M. T. Mehr, and H. Satz, Color screening and deconfinement for bound states of heavy quarks, *Z. Phys. C* **37**, 617 (1988).
- [3] S. Digal, P. Petreczky, and H. Satz, String breaking and quarkonium dissociation at finite temperatures, *Phys. Lett. B* **514**, 57 (2001).
- [4] N. Brambilla *et al.*, Heavy quarkonium: Progress, puzzles, and opportunities, *Eur. Phys. J. C* **71**, 1534 (2011).
- [5] A. Andronic *et al.*, Heavy-flavour and quarkonium production in the LHC era: From proton-proton to heavy-ion collisions, *Eur. Phys. J. C* **76**, 107 (2016).
- [6] R. Rapp and X. Du, Theoretical Perspective on Quarkonia from SPS via RHIC to LHC, *Nucl. Phys. A* **967**, 216 (2017).
- [7] N. Krenz, H. van Hees, and C. Greiner, Quarkonia production in a Langevin approach, *J. Phys.: Conf. Ser.* **1070**, 012008 (2018).
- [8] X. Yao, W. Ke, Y. Xu, S. A. Bass, and B. Müller, Coupled Boltzmann transport equations of heavy quarks and quarkonia in quark-gluon plasma, *J. High Energy Phys.* **01** (2021) 046.
- [9] PHENIX Collaboration, Measurement of $\Upsilon(1S + 2S + 3S)$ production in p+p and Au+Au collisions at $\sqrt{s_{NN}} = 200$ GeV, *Phys. Rev. C* **91**, 024913 (2015).
- [10] STAR Collaboration, Suppression of Υ production in d+Au and Au+Au collisions at $\sqrt{s_{NN}} = 200$ GeV, *Phys. Lett. B* **735**, 127 (2014).
- [11] CMS Collaboration, Measurement of nuclear modification factors of $\Upsilon(1S)$, $\Upsilon(2S)$, and $\Upsilon(3S)$ mesons in PbPb collisions at $\sqrt{s_{NN}} = 5.02$ TeV, *Phys. Lett. B* **790**, 270 (2019).
- [12] CMS Collaboration, Suppression of excited Υ States Relative to the Ground State in PbPb Collisions at $\sqrt{s_{NN}} = 5.02$ TeV, *Phys. Rev. Lett.* **120**, 142301 (2018).
- [13] ALICE Collaboration, Suppression of $\Upsilon(1S)$ at forward rapidity in Pb-Pb collisions at $\sqrt{s_{NN}} = 2.76$ TeV, *Phys. Lett. B* **738**, 361 (2014).
- [14] ALICE Collaboration, $\Upsilon(1S)$ production and nuclear modification at forward rapidity in Pb-Pb collisions at $\sqrt{s_{NN}} = 5.02$ TeV, *Phys. Lett. B* **822**, 136579 (2021).
- [15] STAR Collaboration, Upsilon production in U+U collisions at 193 GeV with the STAR experiment, *Phys. Rev. C* **94**, 064904 (2016).
- [16] STAR Collaboration, Measurement of Sequential Υ Suppression in Au+Au Collisions at $\sqrt{s_{NN}} = 200$ GeV with the STAR Experiment, *Phys. Rev. Lett.* **130**, 112301 (2023).
- [17] NA50 Collaboration, ψ' production in Pb-Pb collisions at 158 GeV/nucleon, *Eur. Phys. J. C* **49**, 559 (2007).
- [18] NA50 Collaboration, A new measurement of J/ψ suppression in Pb-Pb collisions at 158 GeV per nucleon, *Eur. Phys. J. C* **39**, 335 (2005).
- [19] PHENIX Collaboration, J/ψ Production vs Centrality, Transverse Momentum, and Rapidity in Au+Au Collisions at $\sqrt{s_{NN}} = 200$ GeV, *Phys. Rev. Lett.* **98**, 232301 (2007).
- [20] STAR Collaboration, Energy dependence of J/ψ production in Au+Au collisions at $\sqrt{s_{NN}} = 39, 62.4$ and 200 GeV, *Phys. Lett. B* **771**, 13 (2017).
- [21] ATLAS Collaboration, Prompt and non-prompt J/ψ and $\psi(2S)$ suppression at high transverse momentum in 5.02 TeV Pb+Pb collisions with the ATLAS experiment, *Eur. Phys. J. C* **78**, 762 (2018).
- [22] CMS Collaboration, Suppression and azimuthal anisotropy of prompt and nonprompt J/ψ production in PbPb collisions at $\sqrt{s_{NN}} = 2.76$ TeV, *Eur. Phys. J. C* **77**, 252 (2017).
- [23] ALICE Collaboration, Differential studies of inclusive J/ψ and $\psi(2S)$ production at forward rapidity in Pb-Pb collisions at $\sqrt{s_{NN}} = 2.76$ TeV, *J. High Energy Phys.* **05** (2016) 179.
- [24] ATLAS Collaboration, The ATLAS Experiment at the CERN Large Hadron Collider, *JINST* **3**, S08003 (2008).
- [25] ATLAS Collaboration, ATLAS insertable B-layer: Technical design report, ATLAS Report No. ATLAS-TDR-19 and CERN Report No. CERN-LHCC-2010-013, 2010, <https://cds.cern.ch/record/1291633>; Addendum, ATLAS Report No. ATLAS-TDR-19-ADD-1 and CERN Report No. CERN-LHCC-2012-009, 2012, <https://cds.cern.ch/record/1451888>.
- [26] B. Abbott *et al.*, Production and integration of the ATLAS Insertable B-Layer, *J. Inst.* **13**, T05008 (2018).
- [27] ATLAS Collaboration, Performance of the ATLAS trigger system in 2015, *Eur. Phys. J. C* **77**, 317 (2017).
- [28] ATLAS Collaboration, The ATLAS Collaboration software and firmware, ATLAS Report No. ATL-SOFT-PUB-2021-001, 2021, <https://cds.cern.ch/record/2767187>.
- [29] ATLAS Collaboration, Muon reconstruction performance of the ATLAS detector in proton-proton collision data at $\sqrt{s} = 13$ TeV, *Eur. Phys. J. C* **76**, 292 (2016).
- [30] J. Pumplin, D. R. Stump, J. Huston, H.-L. Lai, P. Nadolsky, and W.-K. Tung, New generation of parton distributions with uncertainties from global QCD analysis, *J. High Energy Phys.* **07** (2002) 012.
- [31] T. Sjöstrand, S. Ask, J. R. Christiansen, R. Corke, N. Desai, P. Ilten, S. Mrenna, S. Prestel, C. O. Rasmussen, and P. Z. Skands, An introduction to PYTHIA 8.2, *Comput. Phys. Commun.* **191**, 159 (2015).
- [32] G. T. Bodwin, E. Braaten, and G. P. Lepage, Rigorous QCD analysis of inclusive annihilation and production of heavy quarkonium, *Phys. Rev. D* **51**, 1125 (1995).

- [33] ATLAS Collaboration, The ATLAS Simulation Infrastructure, *Eur. Phys. J. C* **70**, 823 (2010).
- [34] GEANT4 Collaboration, GEANT4: A simulation toolkit, *Nucl. Instrum. Methods Phys. Res., Sect. A* **506**, 250 (2003).
- [35] M. L. Miller, K. Reygiers, S. J. Sanders, and P. Steinberg, Glauber modeling in high-energy nuclear collisions, *Annu. Rev. Nucl. Part. Sci.* **57**, 205 (2007).
- [36] ATLAS Collaboration, Measurement of the $\Upsilon(1S)$ Production Cross-Section in pp Collisions at $\sqrt{s} = 7$ TeV in ATLAS, *Phys. Lett. B* **705**, 9 (2011).
- [37] CMS Collaboration, Measurement of the $\Upsilon(1S)$, $\Upsilon(2S)$ and $\Upsilon(3S)$ Polarizations in pp Collisions at $\sqrt{s} = 7$ TeV, *Phys. Rev. Lett.* **110**, 081802 (2013).
- [38] CMS Collaboration, Measurement of the prompt J/ψ and $\psi(2S)$ polarizations in pp collisions at $\sqrt{s} = 7$ TeV, *Phys. Lett. B* **727**, 381 (2013).
- [39] LHCb Collaboration, Measurement of J/ψ polarization in pp collisions at $\sqrt{s} = 7$ TeV, *Eur. Phys. J. C* **73**, 2631 (2013).
- [40] M. Oreglia, A Study of the Reactions $\psi' \rightarrow \gamma\gamma\psi$, 1980, <https://www.slac.stanford.edu/cgi-wrap/getdoc/slac-r-236.pdf>.
- [41] P. A. Zyla *et al.* (Particle Data Group), Review of Particle Physics, *Prog. Theor. Exp. Phys.* **2020**, 083C01 (2020).
- [42] ATLAS Collaboration, Measurement of quarkonium production in proton–lead and proton–proton collisions at 5.02 TeV with the ATLAS detector, *Eur. Phys. J. C* **78**, 171 (2018).
- [43] ATLAS Collaboration, The simulation principle and performance of the ATLAS fast calorimeter simulation FastCaloSim, ATLAS Report No. ATL-PHYS-PUB-2010-013, 2010, <https://cds.cern.ch/record/1300517>.
- [44] ATLAS Collaboration, Luminosity determination in pp collisions at $\sqrt{s} = 13$ TeV using the ATLAS detector at the LHC, ATLAS Report No. ATLAS-CONF-2019-021, 2019, <https://cds.cern.ch/record/2677054>.
- [45] ATLAS Collaboration, Measurement of the azimuthal anisotropy of charged particles produced in $\sqrt{s_{NN}} = 5.02$ TeV Pb+Pb collisions with the ATLAS detector, *Eur. Phys. J. C* **78**, 997 (2018).
- [46] N. Brambilla, M. A. Escobedo, M. Strickland, A. Vairo, P. V. Griend, and J. H. Weber, Bottomonium production in heavy-ion collisions using quantum trajectories: Differential observables and momentum anisotropy, *Phys. Rev. D* **104**, 094049 (2021).
- [47] X. Du, M. He, and R. Rapp, Color Screening and Regeneration of Bottomonia in High-Energy Heavy-Ion Collisions, *Phys. Rev. C* **96**, 054901 (2017).
- [48] CMS Collaboration, Observation of the $\Upsilon(3S)$ meson and sequential suppression of Υ states in PbPb collisions at $\sqrt{s_{NN}} = 5.02$ TeV, 2022, <https://inspirehep.net/literature/2071548>.
- [49] A. Mocsy, P. Petreczky, and M. Strickland, Quarkonia in the Quark Gluon Plasma, *Int. J. Mod. Phys. A* **28**, 1340012 (2013).
- [50] ATLAS Collaboration, ATLAS computing acknowledgements, ATLAS Report No. ATL-SOFT-PUB-2021-003, 2021, <https://cds.cern.ch/record/2776662>.

G. Aad¹⁰¹, B. Abbott¹¹⁹, D. C. Abbott¹⁰², K. Abeling⁵⁵, S.H. Abidi²⁹, A. Aboulhorma^{35e}, H. Abramowicz¹⁵⁰, H. Abreu¹⁴⁹, Y. Abulaiti¹¹⁶, A. C. Abusleme Hoffman^{136a}, B. S. Acharya^{68a,68b,a}, B. Achkar⁵⁵, L. Adam⁹⁹, C. Adam Bourdarios⁴, L. Adamczyk^{84a}, L. Adamek¹⁵⁴, S. V. Addepalli²⁶, J. Adelman¹¹⁴, A. Adiguzel^{21c}, S. Adorni⁵⁶, T. Auyeub¹³³, A. A. Affolder¹³⁵, Y. Afik³⁶, M. N. Agarar¹³, J. Agarwala^{72a,72b}, A. Aggarwal⁹⁹, C. Agheorghiesei^{27c}, J. A. Aguilar-Saavedra^{129f}, A. Ahmad³⁶, F. Ahmadov^{38,b}, W. S. Ahmed¹⁰³, X. Ai⁴⁸, G. Aielli^{75a,75b}, I. Aizenberg¹⁶⁷, M. Akbiyik⁹⁹, T. P. A. Åkesson⁹⁷, A. V. Akimov³⁷, K. Al Houry⁴¹, G. L. Alberghi^{23b}, J. Albert¹⁶³, P. Albicocco⁵³, M. J. Alconada Verzini⁸⁹, S. Alderweireldt⁵², M. Aleksa³⁶, I. N. Aleksandrov³⁸, C. Alexa^{27b}, T. Alexopoulos¹⁰, A. Alfonsi¹¹³, F. Alfonsi^{23b}, M. Alhroob¹¹⁹, B. Ali¹³¹, S. Ali¹⁴⁷, M. Aliev³⁷, G. Alimonti^{70a}, C. Allaire³⁶, B. M.M. Allbrooke¹⁴⁵, P. P. Allport²⁰, A. Aloisio^{71a,71b}, F. Alonso⁸⁹, C. Alpigiani¹³⁷, E. Alunno Camelia^{75a,75b}, M. Alvarez Estevez⁹⁸, M. G. Alviggi^{71a,71b}, Y. Amaral Coutinho^{81b}, A. Ambler¹⁰³, C. Amelung³⁶, C. G. Ames¹⁰⁸, D. Amidei¹⁰⁵, S. P. Amor Dos Santos^{129a}, S. Amoroso⁴⁸, K. R. Amos¹⁶¹, C. S. Amrouche⁵⁶, V. Ananiev¹²⁴, C. Anastopoulos¹³⁸, N. Andari¹³⁴, T. Andeen¹¹, J. K. Anders¹⁹, S. Y. Andreev^{47a,47b}, A. Andreazza^{70a,70b}, S. Angelidakis⁹, A. Angerami^{41,c}, A. V. Anisenkov³⁷, A. Annovi^{73a}, C. Antel⁵⁶, M. T. Anthony¹³⁸, E. Antipov¹²⁰, M. Antonelli⁵³, D. J.A. Antrim^{17a}, F. Anulli^{74a}, M. Aoki⁸², J. A. Aparisi Pozo¹⁶¹, M. A. Aparo¹⁴⁵, L. Aperio Bella⁴⁸, C. Appelt¹⁸, N. Aranzabal³⁶, V. Araujo Ferraz^{81a}, C. Arcangeletti⁵³, A. T.H. Arce⁵¹, E. Arena⁹¹, J-F. Arguin¹⁰⁷, S. Argyropoulos⁵⁴, J.-H. Arling⁴⁸, A. J. Armbruster³⁶, O. Arnaez¹⁵⁴, H. Arnold¹¹³, Z. P. Arrubarrena Tame¹⁰⁸, G. Artoni^{74a,74b}, H. Asada¹¹⁰, K. Asai¹¹⁷, S. Asai¹⁵², N. A. Asbah⁶¹, E. M. Asimakopoulou¹⁵⁹, J. Assahsah^{35d}, K. Assamagan²⁹, R. Astalos^{28a}, R. J. Atkin^{33a}, M. Atkinson¹⁶⁰, N. B. Atlay¹⁸, H. Atmani^{62b}, P. A. Atmasiddha¹⁰⁵, K. Augsten¹³¹, S. Auricchio^{71a,71b}, A. D. Auriol²⁰, V. A. Austrup¹⁶⁹, G. Avner¹⁴⁹, G. Avolio³⁶, K. Axiotis⁵⁶, M. K. Ayoub^{14c}, G. Azuelos^{107,d}, D. Babal^{28a}, H. Bachacou¹³⁴, K. Bachas^{151,e}, A. Bachiou³⁴, F. Backman^{47a,47b}, A. Badea⁶¹, P. Bagnaia^{74a,74b}, M. Bahmani¹⁸, A. J. Bailey¹⁶¹, V. R. Bailey¹⁶⁰, J. T. Baines¹³³, C. Bakalis¹⁰, O. K. Baker¹⁷⁰, P. J. Bakker¹¹³, E. Bakos¹⁵, D. Bakshi Gupta⁸, S. Balaji¹⁴⁶, R. Balasubramanian¹¹³, E. M. Baldin³⁷, P. Balek¹³², E. Ballabene^{70a,70b}, F. Balli¹³⁴, L. M. Baltes^{63a}, W. K. Balunas³², J. Balz⁹⁹, E. Banas⁸⁵, M. Bandieramonte¹²⁸, A. Bandyopadhyay²⁴, S. Bansal²⁴, L. Barak¹⁵⁰, E. L. Barberio¹⁰⁴, D. Barberis^{57b,57a}, M. Barbero¹⁰¹, G. Barbour⁹⁵, K. N. Barends^{33a}, T. Barillari¹⁰⁹, M-S. Barisits³⁶, J. Barkeloo¹²², T. Barklow¹⁴², R. M. Barnett^{17a}, P. Baron¹²¹, D. A. Baron Moreno¹⁰⁰, A. Baroncelli^{62a}, G. Barone²⁹, A. J. Barr¹²⁵, L. Barranco Navarro^{47a,47b}, F. Barreiro⁹⁸, J. Barreiro Guimarães da Costa^{14a}, U. Barron¹⁵⁰, M. G. Barros Teixeira^{129a}, S. Barsov³⁷, F. Bartels^{63a}, R. Bartoldus¹⁴², A. E. Barton⁹⁰, P. Bartos^{28a}, A. Basalae⁴⁸, A. Basan⁹⁹, M. Baselga⁴⁹, I. Bashta^{76a,76b}

J. Kroll¹²⁷ K. S. Krowpman¹⁰⁶ U. Kruchonak³⁸ H. Krüger²⁴ N. Krumnack⁸⁰ M. C. Kruse⁵¹ J. A. Krzysiak⁸⁵
 A. Kubota¹⁵³ O. Kuchinskaia³⁷ S. Kuday^{3a} D. Kuechler⁴⁸ J. T. Kuechler⁴⁸ S. Kuehn³⁶ T. Kuhl⁴⁸
 V. Kukhtin³⁸ Y. Kulchitsky^{37,m} S. Kuleshov^{136d,136b} M. Kumar^{33g} N. Kumari¹⁰¹ M. Kuna⁶⁰ A. Kupco¹³⁰
 T. Kupfer⁴⁹ A. Kupich³⁷ O. Kuprash⁵⁴ H. Kurashige⁸³ L. L. Kurchaninov^{155a} Y. A. Kurochkin³⁷ A. Kurova³⁷
 E. S. Kuwertz³⁶ M. Kuze¹⁵³ A. K. Kvam¹⁰² J. Kvitá¹²¹ T. Kwan¹⁰³ K. W. Kwok^{64a} C. Lacasta¹⁶¹
 F. Lacava^{74a,74b} H. Lacker¹⁸ D. Lacour¹²⁶ N. N. Lad⁹⁵ E. Ladygin³⁸ B. Laforge¹²⁶ T. Lagouri^{136e} S. Lai⁵⁵
 I. K. Lakomic^{84a} N. Lalloue⁶⁰ J. E. Lambert¹¹⁹ S. Lammers⁶⁷ W. Lampl⁷ C. Lampoudis¹⁵¹
 A. N. Lancaster¹¹⁴ E. Lançon²⁹ U. Landgraf⁵⁴ M. P.J. Landon⁹³ V. S. Lang⁵⁴ R. J. Langenberg¹⁰²
 A. J. Lankford¹⁵⁸ F. Lanni²⁹ K. Lantzsch²⁴ A. Lanza^{72a} A. Lapertosa^{57b,57a} J. F. Laporte¹³⁴ T. Lari^{70a}
 F. Lasagni Manghi^{23b} M. Lassnig³⁶ V. Latonova¹³⁰ T. S. Lau^{64a} A. Laudrain⁹⁹ A. Laurier³⁴ S. D. Lawlor⁹⁴
 Z. Lawrence¹⁰⁰ M. Lazzaroni^{70a,70b} B. Le¹⁰⁰ B. Leban⁹² A. Lebedev⁸⁰ M. LeBlanc³⁶ T. LeCompte⁶
 F. Ledroit-Guillon⁶⁰ A. C.A. Lee⁹⁵ G. R. Lee¹⁶ L. Lee⁶¹ S. C. Lee¹⁴⁷ S. Lee^{47a,47b} L. L. Leeuw^{33c}
 H. P. Lefebvre⁹⁴ M. Lefebvre¹⁶³ C. Leggett^{17a} K. Lehmann¹⁴¹ G. Lehmann Miotto³⁶ W. A. Leight¹⁰²
 A. Leisos^{151,ab} M. A.L. Leite^{81c} C. E. Leitgeb⁴⁸ R. Leitner¹³² K. J.C. Leney⁴⁴ T. Lenz²⁴ S. Leone^{73a}
 C. Leonidopoulos⁵² A. Leopold¹⁴³ C. Leroy¹⁰⁷ R. Les¹⁰⁶ C. G. Lester³² M. Levchenko³⁷ J. Levêque⁴
 D. Levin¹⁰⁵ L. J. Levinson¹⁶⁷ D. J. Lewis²⁰ B. Li^{14b} B. Li^{62b} C. Li^{62a} C-Q. Li^{62c,62d} H. Li^{62a} H. Li^{62b}
 H. Li^{14c} H. Li^{62b} J. Li^{62c} K. Li¹³⁷ L. Li^{62c} M. Li^{14a,14d} Q. Y. Li^{62a} S. Li^{62d,62c,ac} T. Li^{62b} X. Li¹⁰³
 Z. Li^{62b} Z. Li¹²⁵ Z. Li¹⁰³ Z. Li⁹¹ Z. Liang^{14a} M. Liberatore⁴⁸ B. Liberti^{75a} K. Lie^{64c} J. Lieber Marin^{81b}
 K. Lin¹⁰⁶ R. A. Linck⁶⁷ R. E. Lindley⁷ J. H. Lindon² A. Linss⁴⁸ E. Lipeles¹²⁷ A. Lipniacka¹⁶
 T. M. Liss^{160,ad} A. Lister¹⁶² J. D. Little⁴ B. Liu^{14a} B. X. Liu¹⁴¹ D. Liu^{62d,62c} J. B. Liu^{62a} J. K.K. Liu³²
 K. Liu^{62d,62c} M. Liu^{62a} M. Y. Liu^{62a} P. Liu^{14a} Q. Liu^{62d,137,62c} X. Liu^{62a} Y. Liu⁴⁸ Y. Liu^{14c,14d}
 Y. L. Liu¹⁰⁵ Y. W. Liu^{62a} M. Livan^{72a,72b} J. Llorente Merino¹⁴¹ S. L. Lloyd⁹³ E. M. Lobodzinska⁴⁸ P. Loch⁷
 S. Loffredo^{75a,75b} T. Lohse¹⁸ K. Lohwasser¹³⁸ M. Lokajicek¹³⁰ J. D. Long¹⁶⁰ I. Longarini^{74a,74b}
 L. Longo^{69a,69b} R. Longo¹⁶⁰ I. Lopez Paz³⁶ A. Lopez Solis⁴⁸ J. Lorenz¹⁰⁸ N. Lorenzo Martinez⁴
 A. M. Lory¹⁰⁸ A. Lösle⁵⁴ X. Lou^{47a,47b} X. Lou^{14a,14d} A. Lounis⁶⁶ J. Love⁶ P. A. Love⁹⁰
 J. J. Lozano Bahilo¹⁶¹ G. Lu^{14a,14d} M. Lu⁷⁹ S. Lu¹²⁷ Y. J. Lu⁶⁵ H. J. Lubatti¹³⁷ C. Luci^{74a,74b}
 F. L. Lucio Alves^{14c} A. Lucotte⁶⁰ F. Luehring⁶⁷ I. Luise¹⁴⁴ O. Lukianchuk⁶⁶ O. Lundberg¹⁴³
 B. Lund-Jensen¹⁴³ N. A. Luongo¹²² M. S. Lutz¹⁵⁰ D. Lynn²⁹ H. Lyons⁹¹ R. Lysak¹³⁰ E. Lytken⁹⁷ F. Lyu^{14a}
 V. Lyubushkin³⁸ T. Lyubushkina³⁸ H. Ma²⁹ L. L. Ma^{62b} Y. Ma⁹⁵ D. M. Mac Donell¹⁶³ G. Maccarrone⁵³
 J. C. MacDonald¹³⁸ R. Madar⁴⁰ W. F. Mader⁵⁰ J. Maeda⁸³ T. Maeno²⁹ M. Maerker⁵⁰ V. Magerl⁵⁴
 J. Magro^{68a,68c} H. Maguire¹³⁸ D. J. Mahon⁴¹ C. Maidantchik^{81b} A. Maio^{129a,129b,129d} K. Maj^{84a}
 O. Majersky^{28a} S. Majewski¹²² N. Makovec⁶⁶ V. Maksimovic¹⁵ B. Malaescu¹²⁶ Pa. Malecki⁸⁵ V. P. Maleev³⁷
 F. Malek⁶⁰ D. Malito^{43b,43a} U. Mallik⁷⁹ C. Malone³² S. Maltezos¹⁰ S. Malyukov³⁸ J. Mamuzic¹¹⁹ G. Mancini⁵³
 G. Manco^{72a,72b} J. P. Mandalia⁹³ I. Mandić⁹² L. Manhaes de Andrade Filho^{81a} I. M. Maniatis¹⁵¹ M. Manisha¹³⁴
 J. Manjarres Ramos⁵⁰ D. C. Mankad¹⁶⁷ K. H. Mankinen⁹⁷ A. Mann¹⁰⁸ A. Manousos⁷⁸ B. Mansoulie¹³⁴
 S. Manzoni³⁶ A. Marantis¹⁵¹ G. Marchiori⁵ M. Marcisovsky¹³⁰ L. Marcoccia^{75a,75b} C. Marcon⁹⁷
 M. Marinescu²⁰ M. Marjanovic¹¹⁹ Z. Marshall^{17a} S. Marti-Garcia¹⁶¹ T. A. Martin¹⁶⁵ V. J. Martin⁵²
 B. Martin dit Latour¹⁶ L. Martinelli^{74a,74b} M. Martinez^{13,w} P. Martinez Agullo¹⁶¹ V. I. Martinez Outschoorn¹⁰²
 P. Martinez Suarez¹³ S. Martin-Haugh¹³³ V. S. Martoiu^{27b} A. C. Martyniuk⁹⁵ A. Marzin³⁶ S. R. Maschek¹⁰⁹
 L. Masetti⁹⁹ T. Mashimo¹⁵² J. Masik¹⁰⁰ A. L. Maslennikov³⁷ L. Massa^{23b} P. Massarotti^{71a,71b}
 P. Mastrandrea^{73a,73b} A. Mastroberardino^{43b,43a} T. Masubuchi¹⁵² T. Mathisen¹⁵⁹ A. Matic¹⁰⁸ N. Matsuzawa¹⁵²
 J. Maurer^{27b} B. Maček⁹² D. A. Maximov³⁷ R. Mazini¹⁴⁷ I. Maznas¹⁵¹ M. Mazza¹⁰⁶ S. M. Mazza¹³⁵
 C. Mc Ginn^{29,h} J. P. Mc Gowan¹⁰³ S. P. Mc Kee¹⁰⁵ T. G. McCarthy¹⁰⁹ W. P. McCormack^{17a} E. F. McDonald¹⁰⁴
 A. E. McDougall¹¹³ J. A. Mcfayden¹⁴⁵ G. Mchedlidze^{148b} R. P. Mckenzie^{33g} T. C. McLachlan⁴⁸
 D. J. McLaughlin⁹⁵ K. D. McLean¹⁶³ S. J. McMahan¹³³ P. C. McNamara¹⁰⁴ R. A. McPherson^{163,q}
 J. E. Mdhluli^{33g} S. Meehan³⁶ T. Megy⁴⁰ S. Mehlhase¹⁰⁸ A. Mehta⁹¹ B. Meirose⁴⁵ D. Melini¹⁴⁹
 B. R. Mellado Garcia^{33g} A. H. Melo⁵⁵ F. Meloni⁴⁸ E. D. Mendes Gouveia^{129a} A. M. Mendes Jacques Da Costa²⁰
 H. Y. Meng¹⁵⁴ L. Meng⁹⁰ S. Menke¹⁰⁹ M. Mentink³⁶ E. Meoni^{43b,43a} C. Merlassino¹²⁵ L. Merola^{71a,71b}
 C. Meroni^{70a} G. Merz¹⁰⁵ O. Meshkov³⁷ J. K.R. Meshreki¹⁴⁰ J. Metcalfe⁶ A. S. Mete⁶ C. Meyer⁶⁷
 J-P. Meyer¹³⁴ M. Michetti¹⁸ R. P. Middleton¹³³ L. Mijović⁵² G. Mikenberg¹⁶⁷ M. Mikesikova¹³⁰
 M. Mikuž⁹² H. Mildner¹³⁸ A. Milic¹⁵⁴ C. D. Milke⁴⁴ D. W. Miller³⁹ L. S. Miller³⁴ A. Milov¹⁶⁷
 D. A. Milstead^{47a,47b} T. Min^{14c} A. A. Minaenko³⁷ I. A. Minashvili^{148b} L. Mince⁵⁹ A. I. Mincer¹¹⁶ B. Mindur^{84a}
 M. Mineev³⁸ Y. Minegishi¹⁵² Y. Mino⁸⁶ L. M. Mir¹³ M. Miralles Lopez¹⁶¹ M. Mironova¹²⁵ T. Mitani¹⁶⁶
 A. Mitra¹⁶⁵ V. A. Mitsou¹⁶¹ O. Miu¹⁵⁴ P. S. Miyagawa⁹³ Y. Miyazaki⁸⁸ A. Mizukami⁸² J. U. Mjörnmark⁹⁷
 T. Mkrtchyan^{63a} M. Mlynarikova¹¹⁴ T. Moa^{47a,47b} S. Mobius⁵⁵ K. Mochizuki¹⁰⁷ P. Moder⁴⁸ P. Mogg¹⁰⁸
 A. F. Mohammed^{14a,14d} S. Mohapatra⁴¹ G. Mokgatitwane^{33g} B. Mondal¹⁴⁰ S. Mondal¹³¹ K. Mönig⁴⁸
 E. Monnier¹⁰¹ L. Monsonis Romero¹⁶¹ J. Montejo Berlingen³⁶ M. Montella¹¹⁸ F. Monticelli⁸⁹ N. Morange⁶⁶
 A. L. Moreira De Carvalho^{129a} M. Moreno Llácer¹⁶¹ C. Moreno Martinez¹³ P. Morettini^{57b} S. Morgenstern¹⁶⁵

- M. Morii ⁶¹, M. Morinaga ¹⁵², V. Morisbak ¹²⁴, A. K. Morley ³⁶, F. Morodei ^{74a,74b}, L. Morvaj ³⁶, P. Moschovakos ³⁶,
 B. Moser ³⁶, M. Mosidze ^{148b}, T. Moskalets ⁵⁴, P. Moskvitina ¹¹², J. Moss ^{31,ae}, E. J.W. Moyses ¹⁰², S. Muanza ¹⁰¹,
 J. Mueller ¹²⁸, D. Muenstermann ⁹⁰, R. Müller ¹⁹, G. A. Mullier ⁹⁷, J. J. Mullin ¹²⁷, D. P. Mungo ^{70a,70b},
 J. L. Munoz Martinez ¹³, D. Munoz Perez ¹⁶¹, F. J. Munoz Sanchez ¹⁰⁰, M. Murin ¹⁰⁰, W. J. Murray ^{165,133},
 A. Murrone ^{70a,70b}, J. M. Muse ¹¹⁹, M. Muškinja ^{17a}, C. Mwewa ²⁹, A. G. Myagkov ^{37,m}, A. J. Myers ⁸,
 A. A. Myers ¹²⁸, G. Myers ⁶⁷, M. Myska ¹³¹, B. P. Nachman ^{17a}, O. Nackenhorst ⁴⁹, A. Nag ⁵⁰, K. Nagai ¹²⁵,
 K. Nagano ⁸², J. L. Nagle ^{29,h}, E. Nagy ¹⁰¹, A. M. Nairz ³⁶, Y. Nakahama ⁸², K. Nakamura ⁸², H. Nanjo ¹²³,
 R. Narayan ⁴⁴, E. A. Narayanan ¹¹¹, I. Naryshkin ³⁷, M. Naseri ³⁴, C. Nass ²⁴, G. Navarro ^{22a},
 J. Navarro-Gonzalez ¹⁶¹, R. Nayak ¹⁵⁰, P. Y. Nechaeva ³⁷, F. Nechansky ⁴⁸, T. J. Neep ²⁰, A. Negri ^{72a,72b},
 M. Negrini ^{23b}, C. Nellist ¹¹², C. Nelson ¹⁰³, K. Nelson ¹⁰⁵, S. Nemecek ¹³⁰, M. Nessi ^{36,af}, M. S. Neubauer ¹⁶⁰,
 F. Neuhaus ⁹⁹, J. Neundorff ⁴⁸, R. Newhouse ¹⁶², P. R. Newman ²⁰, C. W. Ng ¹²⁸, Y. S. Ng ¹⁸, Y. W.Y. Ng ¹⁵⁸,
 B. Ngair ^{35e}, H. D.N. Nguyen ¹⁰⁷, R. B. Nickerson ¹²⁵, R. Nicolaidou ¹³⁴, J. Nielsen ¹³⁵, M. Niemeyer ⁵⁵,
 N. Nikiforou ³⁶, V. Nikolaenko ^{37,m}, I. Nikolic-Audit ¹²⁶, K. Nikolopoulos ²⁰, P. Nilsson ²⁹, H. R. Nindhito ⁵⁶,
 A. Nisati ^{74a}, N. Nishu ², R. Nisius ¹⁰⁹, J-E. Nitschke ⁵⁰, E. K. Nkadimeng ^{33g}, S. J. Noacco Rosende ⁸⁹, T. Nobe ¹⁵²,
 D. L. Noel ³², Y. Noguchi ⁸⁶, T. Nommensen ¹⁴⁶, M. A. Nomura ²⁹, M. B. Norfolk ¹³⁸, R. R.B. Norisam ⁹⁵,
 B. J. Norman ³⁴, J. Novak ⁹², T. Novak ⁴⁸, O. Novgorodova ⁵⁰, L. Novotny ¹³¹, R. Novotny ¹¹¹, L. Nozka ¹²¹,
 K. Ntekas ¹⁵⁸, E. Nurse ⁹⁵, F. G. Oakham ^{34,d}, J. Ocariz ¹²⁶, A. Ochi ⁸³, I. Ochoa ^{129a}, S. Oda ⁸⁸, S. Oerdek ¹⁵⁹,
 A. Ogrodnik ^{84a}, A. Oh ¹⁰⁰, C. C. Ohm ¹⁴³, H. Oide ¹⁵³, R. Oishi ¹⁵², M. L. Ojeda ⁴⁸, Y. Okazaki ⁸⁶, M. W. O'Keefe ⁹¹,
 Y. Okumura ¹⁵², A. Olariu ^{27b}, L. F. Oleiro Seabra ^{129a}, S. A. Olivares Pino ^{136e}, D. Oliveira Damazio ²⁹,
 D. Oliveira Goncalves ^{81a}, J. L. Oliver ¹⁵⁸, M. J.R. Olsson ¹⁵⁸, A. Olszewski ⁸⁵, J. Olszowska ^{85,j}, Ö. O. Öncel ⁵⁴,
 D. C. O'Neil ¹⁴¹, A. P. O'Neill ¹⁹, A. Onofre ^{129a,129e}, P. U.E. Onyisi ¹¹, M. J. Oreglia ³⁹, G. E. Orellana ⁸⁹,
 D. Orestano ^{76a,76b}, N. Orlando ¹³, R. S. Orr ¹⁵⁴, V. O'Shea ⁵⁹, R. Ospanov ^{62a}, G. Otero y Garzon ³⁰, H. Otono ⁸⁸,
 P. S. Ott ^{63a}, G. J. Ottino ^{17a}, M. Ouchrif ^{35d}, J. Ouellette ^{29,h}, F. Ould-Saada ¹²⁴, M. Owen ⁵⁹, R. E. Owen ¹³³,
 K. Y. Oyulmaz ^{21a}, V. E. Ozcan ^{21a}, N. Ozturk ⁸, S. Ozturk ^{21d}, J. Pacalt ¹²¹, H. A. Pacey ³², K. Pachal ⁵¹,
 A. Pacheco Pages ¹³, C. Padilla Aranda ¹³, G. Padovano ^{174a,74b}, S. Pagan Griso ^{17a}, G. Palacino ⁶⁷, A. Palazzo ^{69a,69b},
 S. Palazzo ⁵², S. Palestini ³⁶, M. Palka ^{84b}, J. Pan ¹⁷⁰, D. K. Panchal ¹¹, C. E. Pandini ¹¹³, J. G. Panduro Vazquez ⁹⁴,
 P. Pani ⁴⁸, G. Panizzo ^{68a,68c}, L. Paolozzi ⁵⁶, C. Papadatos ¹⁰⁷, S. Parajuli ⁴⁴, A. Paramonov ⁶, C. Paraskevopoulos ¹⁰,
 D. Paredes Hernandez ^{64b}, T. H. Park ¹⁵⁴, M. A. Parker ³², F. Parodi ^{57b,57a}, E. W. Parrish ¹¹⁴, V. A. Parrish ⁵²,
 J. A. Parsons ⁴¹, U. Parzefall ⁵⁴, B. Pascual Dias ¹⁰⁷, L. Pascual Dominguez ¹⁵⁰, V. R. Pascuzzi ^{17a}, F. Pasquali ¹¹³,
 E. Pasqualucci ^{74a}, S. Passaggio ^{57b}, F. Pastore ⁹⁴, P. Pasuwan ^{47a,47b}, J. R. Pater ¹⁰⁰, J. Patton ⁹¹, T. Pauly ³⁶,
 J. Parkes ¹⁴², M. Pedersen ¹²⁴, R. Pedro ^{129a}, S. V. Peleganchuk ³⁷, O. Penc ¹³⁰, C. Peng ^{64b}, H. Peng ^{62a},
 M. Penzin ³⁷, B. S. Peralva ^{81a}, A. P. Pereira Peixoto ⁶⁰, L. Pereira Sanchez ^{47a,47b}, D. V. Perepelitsa ^{29,h},
 E. Perez Codina ^{155a}, M. Perganti ¹⁰, L. Perini ^{70a,70b,j}, H. Pernegger ³⁶, S. Perrella ³⁶, A. Perrevoort ¹¹², O. Perrin ⁴⁰,
 K. Peters ⁴⁸, R. F.Y. Peters ¹⁰⁰, B. A. Petersen ³⁶, T. C. Petersen ⁴², E. Petit ¹⁰¹, V. Petousis ¹³¹, C. Petridou ¹⁵¹,
 A. Petrukhin ¹⁴⁰, M. Pettee ^{17a}, N. E. Pettersson ³⁶, A. Petukhov ³⁷, K. Petukhova ¹³², A. Peyaud ¹³⁴, R. Pezoa ^{136f},
 L. Pezzotti ³⁶, G. Pezzullo ¹⁷⁰, T. Pham ¹⁰⁴, P. W. Phillips ¹³³, M. W. Phipps ¹⁶⁰, G. Piacquadio ¹⁴⁴, E. Pianori ^{17a},
 F. Piazza ^{70a,70b}, R. Piegaia ³⁰, D. Pietreanu ^{27b}, A. D. Pilkington ¹⁰⁰, M. Pinamonti ^{68a,68c}, J. L. Pinfold ²,
 B. C. Pinheiro Pereira ^{129a}, C. Pitman Donaldson ⁹⁵, D. A. Pizzi ³⁴, L. Pizzimento ^{75a,75b}, A. Pizzini ¹¹³, M.-A. Pleier ²⁹,
 V. Plesanovs ⁵⁴, V. Pleskot ¹³², E. Plotnikova ³⁸, G. Poddar ⁴, R. Poettgen ⁹⁷, R. Poggi ⁵⁶, L. Poggioli ¹²⁶,
 I. Pogrebnyak ¹⁰⁶, D. Pohl ²⁴, I. Pokharel ⁵⁵, S. Polacek ¹³², G. Polesello ^{72a}, A. Poley ^{141,155a}, R. Polifka ¹³¹,
 A. Polini ^{23b}, C. S. Pollard ¹²⁵, Z. B. Pollock ¹¹⁸, V. Polychronakos ²⁹, D. Ponomarenko ³⁷, L. Pontecorvo ³⁶,
 S. Popa ^{27a}, G. A. Popeneciu ^{27d}, D. M. Portillo Quintero ^{155a}, S. Pospisil ¹³¹, P. Postolache ^{27c}, K. Potamianos ¹²⁵,
 I. N. Potrap ³⁸, C. J. Potter ³², H. Potti ¹, T. Poulsen ⁴⁸, J. Poveda ¹⁶¹, G. Pownall ⁴⁸, M. E. Pozo Astigarraga ³⁶,
 A. Prades Ibanez ¹⁶¹, M. M. Prapa ⁴⁶, D. Price ¹⁰⁰, M. Primavera ^{69a}, M. A. Principe Martin ⁹⁸, M. L. Proffitt ¹³⁷,
 N. Proklova ³⁷, K. Prokofiev ^{64c}, G. Proto ^{75a,75b}, S. Protopopescu ²⁹, J. Proudfoot ⁶, M. Przybycien ^{84a},
 J. E. Pudefoot ¹³⁸, D. Pudzha ³⁷, P. Puzo ⁶⁶, D. Pyatizbyantseva ³⁷, J. Qian ¹⁰⁵, Y. Qin ¹⁰⁰, T. Qiu ⁹³, A. Quadri ⁵⁵,
 M. Queitsch-Maitland ²⁴, G. Rabanal Bolanos ⁶¹, D. Rafanoharana ⁵⁴, F. Ragusa ^{70a,70b}, J. L. Rainbolt ³⁹,
 J. A. Raine ⁵⁶, S. Rajagopalan ²⁹, E. Ramakoti ³⁷, K. Ran ^{14a,14d}, V. Raskina ¹²⁶, D. F. Rassloff ^{63a}, S. Rave ⁹⁹,
 B. Ravina ⁵⁹, I. Ravinovich ¹⁶⁷, M. Raymond ³⁶, A. L. Read ¹²⁴, N. P. Readoff ¹³⁸, D. M. Rebuffi ^{72a,72b},
 G. Redlinger ²⁹, K. Reeves ⁴⁵, J. A. Reidelsturz ¹⁶⁹, D. Reikher ¹⁵⁰, A. Reiss ⁹⁹, A. Rej ¹⁴⁰, C. Rembser ³⁶,
 A. Renardi ⁴⁸, M. Renda ^{27b}, M. B. Rendel ¹⁰⁹, A. G. Rennie ⁵⁹, S. Resconi ^{70a}, M. Ressegotti ^{57b,57a},
 E. D. Resseguie ^{17a}, S. Rettie ⁹⁵, B. Reynolds ¹¹⁸, E. Reynolds ^{17a}, M. Rezaei Estabragh ¹⁶⁹, O. L. Rezanova ³⁷,
 P. Reznicek ¹³², E. Ricci ^{77a,77b}, R. Richter ¹⁰⁹, S. Richter ^{47a,47b}, E. Richter-Was ^{84b}, M. Ridel ¹²⁶, P. Rieck ¹¹⁶,
 P. Riedler ³⁶, M. Rijssenbeek ¹⁴⁴, A. Rimoldi ^{72a,72b}, M. Rimoldi ⁴⁸, L. Rinaldi ^{23b,23a}, T. T. Rinn ²⁹,
 M. P. Rinnagel ¹⁰⁸, G. Ripellino ¹⁴³, I. Riu ¹³, P. Rivadeneira ⁴⁸, J. C. Rivera Vergara ¹⁶³, F. Rizatdinova ¹²⁰,
 E. Rizvi ⁹³, C. Rizzi ⁵⁶, B. A. Roberts ¹⁶⁵, B. R. Roberts ^{17a}, S. H. Robertson ^{103,q}, M. Robin ⁴⁸, D. Robinson ³²,
 C. M. Robles Gajardo ^{136f}, M. Robles Manzano ⁹⁹, A. Robson ⁵⁹, A. Rocchi ^{75a,75b}, C. Roda ^{73a,73b},
 S. Rodriguez Bosca ^{63a}, Y. Rodriguez Garcia ^{22a}, A. Rodriguez Rodriguez ⁵⁴, A. M. Rodríguez Vera ^{155b}, S. Roe ³⁶

- J. T. Roemer¹⁵⁸, A. R. Roepe-Gier¹¹⁹, J. Roggel¹⁶⁹, O. Røhne¹²⁴, R. A. Rojas¹⁶³, B. Roland⁵⁴, C. P.A. Roland⁶⁷, J. Roloff²⁹, A. Romaniouk³⁷, E. Romano^{72a,72b}, M. Romano^{23b}, A. C. Romero Hernandez¹⁶⁰, N. Rompotis⁹¹, L. Roos¹²⁶, S. Rosati^{74a}, B. J. Rosser³⁹, E. Rossi⁴, E. Rossi^{71a,71b}, L. P. Rossi^{57b}, L. Rossini⁴⁸, R. Rosten¹¹⁸, M. Rotaru^{27b}, B. Rottler⁵⁴, D. Rousseau⁶⁶, D. Rousso³², G. Rovelli^{72a,72b}, A. Roy¹⁶⁰, A. Rozanov¹⁰¹, Y. Rozen¹⁴⁹, X. Ruan^{33g}, A. Rubio Jimenez¹⁶¹, A. J. Ruby⁹¹, T. A. Ruggeri¹, F. Rühr⁵⁴, A. Ruiz-Martinez¹⁶¹, A. Rummler³⁶, Z. Rurikova⁵⁴, N. A. Rusakovich³⁸, H. L. Russell¹⁶³, J. P. Rutherford⁷, E. M. Rüttinger¹³⁸, K. Rybacki⁹⁰, M. Rybar¹³², E. B. Rye¹²⁴, A. Ryzhov³⁷, J. A. Sabater Iglesias⁵⁶, P. Sabatini¹⁶¹, L. Sabetta^{74a,74b}, H.F.-W. Sadrozinski¹³⁵, F. Safai Tehrani^{74a}, B. Safarzadeh Samani¹⁴⁵, M. Safdari¹⁴², S. Saha¹⁰³, M. Sahinsky¹⁰⁹, M. Saimpert¹³⁴, M. Saito¹⁵², T. Saito¹⁵², D. Salamani³⁶, G. Salamanna^{76a,76b}, A. Salnikov¹⁴², J. Salt¹⁶¹, A. Salvador Salas¹³, D. Salvatore^{43b,43a}, F. Salvatore¹⁴⁵, A. Salzburger³⁶, D. Sammel⁵⁴, D. Sampsonidis¹⁵¹, D. Sampsonidou^{62d,62c}, J. Sánchez¹⁶¹, A. Sanchez Pineda⁴, V. Sanchez Sebastian¹⁶¹, H. Sandaker¹²⁴, C. O. Sander⁴⁸, J. A. Sandesara¹⁰², M. Sandhoff¹⁶⁹, C. Sandoval^{22b}, D. P.C. Sankey¹³³, A. Sansoni⁵³, L. Santi^{74a,74b}, C. Santoni⁴⁰, H. Santos^{129a,129b}, S. N. Santpur^{17a}, A. Santra¹⁶⁷, K. A. Saoucha¹³⁸, J. G. Saraiva^{129a,129d}, J. Sardain¹⁰¹, O. Sasaki⁸², K. Sato¹⁵⁶, C. Sauer^{63b}, F. Sauerburger⁵⁴, E. Sauvan⁴, P. Savard^{154,d}, R. Sawada¹⁵², C. Sawyer¹³³, L. Sawyer⁹⁶, I. Sayago Galvan¹⁶¹, C. Sbarra^{23b}, A. Sbrizzi^{23b,23a}, T. Scanlon⁹⁵, J. Schaarschmidt¹³⁷, P. Schacht¹⁰⁹, D. Schaefer³⁹, U. Schäfer⁹⁹, A. C. Schaffer⁶⁶, D. Schaile¹⁰⁸, R. D. Schamberger¹⁴⁴, E. Schanet¹⁰⁸, C. Scharf¹⁸, V. A. Schegelsky³⁷, D. Scheirich¹³², F. Schenck¹⁸, M. Schernau¹⁵⁸, C. Scheulen⁵⁵, C. Schiavi^{57b,57a}, Z. M. Schillaci²⁶, E. J. Schioppa^{69a,69b}, M. Schioppa^{43b,43a}, B. Schlag⁹⁹, K. E. Schleicher⁵⁴, S. Schlenker³⁶, K. Schmieden⁹⁹, C. Schmitt⁹⁹, S. Schmitt⁴⁸, L. Schoeffel¹³⁴, A. Schoening^{63b}, P. G. Scholer⁵⁴, E. Schopf¹²⁵, M. Schott⁹⁹, J. Schovancova³⁶, S. Schramm⁵⁶, F. Schroeder¹⁶⁹, H.-C. Schultz-Coulon^{63a}, M. Schumacher⁵⁴, B. A. Schumm¹³⁵, Ph. Schune¹³⁴, A. Schwartzman¹⁴², T. A. Schwarz¹⁰⁵, Ph. Schwemling¹³⁴, R. Schwienhorst¹⁰⁶, A. Sciandra¹³⁵, G. Sciolla²⁶, F. Scuri^{73a}, F. Scutti¹⁰⁴, C. D. Sebastiani⁹¹, K. Sedlaczek⁴⁹, P. Seema¹⁸, S. C. Seidel¹¹¹, A. Seiden¹³⁵, B. D. Seidlitz⁴¹, T. Seiss³⁹, C. Seitz⁴⁸, J. M. Seixas^{81b}, G. Sekhniaidze^{71a}, S. J. Sekula⁴⁴, L. Selem⁴, N. Semprini-Cesari^{23b,23a}, S. Sen⁵¹, V. Senthilkumar¹⁶¹, L. Serin⁶⁶, L. Serkin^{68a,68b}, M. Sessa^{76a,76b}, H. Severini¹¹⁹, S. Sevova¹⁴², F. Sforza^{57b,57a}, A. Sfyrila⁵⁶, E. Shabalina⁵⁵, R. Shaheen¹⁴³, J. D. Shahinian¹²⁷, N. W. Shaikh^{47a,47b}, D. Shaked Renous¹⁶⁷, L. Y. Shan^{14a}, M. Shapiro^{17a}, A. Sharma³⁶, A. S. Sharma¹⁶², P. Sharma⁷⁹, S. Sharma⁴⁸, P. B. Shatalov³⁷, K. Shaw¹⁴⁵, S. M. Shaw¹⁰⁰, Q. Shen^{62c}, P. Sherwood⁹⁵, L. Shi⁹⁵, C. O. Shimmin¹⁷⁰, Y. Shimogama¹⁶⁶, J. D. Shinner⁹⁴, I. P.J. Shipsey¹²⁵, S. Shirabe⁶⁰, M. Shiyakova³⁸, J. Shlomi¹⁶⁷, M. J. Shochet³⁹, J. Shojaii¹⁰⁴, D. R. Shope¹⁴³, S. Shrestha¹¹⁸, E. M. Shrif^{33g}, M. J. Shroff¹⁶³, P. Sicho¹³⁰, A. M. Sickles¹⁶⁰, E. Sideras Haddad^{33g}, O. Sidiropoulou³⁶, A. Sidoti^{23b}, F. Siegert⁵⁰, Dj. Sijacki¹⁵, R. Sikora^{84a}, F. Sili⁸⁹, J. M. Silva²⁰, M. V. Silva Oliveira³⁶, S. B. Silverstein^{47a}, S. Simion⁶⁶, R. Simoniello³⁶, E. L. Simpson⁵⁹, N. D. Simpson⁹⁷, S. Simsek^{21d}, S. Sindhu⁵⁵, P. Sinervo¹⁵⁴, V. Sinetckii³⁷, S. Singh¹⁴¹, S. Singh¹⁵⁴, S. Sinha⁴⁸, S. Sinha^{33g}, M. Sioli^{23b,23a}, I. Siral¹²², S. Yu. Sivoklokov^{37,j}, J. Sjölin^{47a,47b}, A. Skaf⁵⁵, E. Skorda⁹⁷, P. Skubic¹¹⁹, M. Slawinska⁸⁵, V. Smakhtin¹⁶⁷, B. H. Smart¹³³, J. Smiesko¹³², S. Yu. Smirnov³⁷, Y. Smirnov³⁷, L. N. Smirnova^{37,m}, O. Smirnova⁹⁷, E. A. Smith³⁹, H. A. Smith¹²⁵, J. L. Smith⁹¹, R. Smith¹⁴², M. Smizanska⁹⁰, K. Smolek¹³¹, A. Smykiewicz⁸⁵, A. A. Snesarev³⁷, H. L. Snoek¹¹³, S. Snyder²⁹, R. Sobie^{163,q}, A. Soffer¹⁵⁰, C. A. Solans Sanchez³⁶, E. Yu. Soldatov³⁷, U. Soldevila¹⁶¹, A. A. Solodkov³⁷, S. Solomon⁵⁴, A. Soloshenko³⁸, K. Solovieva⁵⁴, O. V. Solovyanov³⁷, V. Solovveyev³⁷, P. Sommer³⁶, A. Sonay¹³, W. Y. Song^{155b}, A. Sopcak¹³¹, A. L. Soppio⁹⁵, F. Sopkova^{28b}, V. Sothilingam^{63a}, S. Sottocornola^{72a,72b}, R. Soualah^{115c}, Z. Soumami^{35e}, D. South⁴⁸, S. Spagnolo^{69a,69b}, M. Spalla¹⁰⁹, F. Spanò⁹⁴, D. Sperlich⁵⁴, G. Spigo³⁶, M. Spina¹⁴⁵, S. Spinali⁹⁰, D. P. Spiteri⁵⁹, M. Spousta¹³², E. J. Staats³⁴, A. Stabile^{70a,70b}, R. Stamen^{63a}, M. Stamenkovic¹¹³, A. Stampekis²⁰, M. Standke²⁴, E. Stanecka⁸⁵, B. Stanislaus^{17a}, M. M. Stanitzki⁴⁸, M. Stankaityte¹²⁵, B. Stapf⁴⁸, E. A. Starchenko³⁷, G. H. Stark¹³⁵, J. Stark¹⁰¹, D. M. Starke^{155b}, P. Staroba¹³⁰, P. Starovoitov^{63a}, S. Stärz¹⁰³, R. Staszewski⁸⁵, G. Stavropoulos⁴⁶, J. Steentoft¹⁵⁹, P. Steinberg²⁹, A. L. Steinhebel¹²², B. Stelzer^{141,155a}, H. J. Stelzer¹²⁸, O. Stelzer-Chilton^{155a}, H. Stenzel⁵⁸, T. J. Stevenson¹⁴⁵, G. A. Stewart³⁶, M. C. Stockton³⁶, G. Stoica^{27b}, M. Stolarski^{129a}, S. Stojek¹⁰⁹, A. Straessner⁵⁰, J. Strandberg¹⁴³, S. Strandberg^{47a,47b}, M. Strauss¹¹⁹, T. Streblner¹⁰¹, P. Striznec^{28b}, R. Ströhmer¹⁶⁴, D. M. Strom¹²², L. R. Strom⁴⁸, R. Stroynowski⁴⁴, A. Strubig^{47a,47b}, S. A. Stucci²⁹, B. Stugu¹⁶, J. Stupak¹¹⁹, N. A. Styles⁴⁸, D. Su¹⁴², S. Su^{62a}, W. Su^{62d,137,62c}, X. Su^{62a,66}, K. Sugizaki¹⁵², V. V. Sulim³⁷, M. J. Sullivan⁹¹, D. M.S. Sultan^{77a,77b}, L. Sultanaliyeva³⁷, S. Sultansoy^{3b}, T. Sumida⁸⁶, S. Sun¹⁰⁵, S. Sun¹⁶⁸, O. Sunneborn Gudnadottir¹⁵⁹, M. R. Sutton¹⁴⁵, M. Svatos¹³⁰, M. Swiatlowski^{155a}, T. Swirski¹⁶⁴, I. Sykora^{28a}, M. Sykora¹³², T. Sykora¹³², D. Ta⁹⁹, K. Tackmann^{48,ag}, A. Taffard¹⁵⁸, R. Tafirout^{155a}, J. S. Tafuya Vargas⁶⁶, R. H.M. Taibah¹²⁶, R. Takashima⁸⁷, K. Takeda⁸³, E. P. Takeva⁵², Y. Takubo⁸², M. Talby¹⁰¹, A. A. Talyshev³⁷, K. C. Tam^{64b}, N. M. Tamir¹⁵⁰, A. Tanaka¹⁵², J. Tanaka¹⁵², R. Tanaka⁶⁶, M. Tanasini^{57b,57a}, J. Tang^{62c}, Z. Tao¹⁶², S. Tapia Araya⁸⁰, S. Tapprogge⁹⁹, A. Tarek Abouelfadl Mohamed¹⁰⁶, S. Tarem¹⁴⁹, K. Tariq^{62b}, G. Tarna^{27b}, G. F. Tartarelli^{70a}, P. Tas¹³², M. Tasevsky¹³⁰, E. Tassi^{43b,43a}, A. C. Tate¹⁶⁰, G. Tateno¹⁵², Y. Tayalati^{35e}, G. N. Taylor¹⁰⁴, W. Taylor^{155b}, H. Teagle⁹¹, A. S. Tee¹⁶⁸, R. Teixeira De Lima¹⁴², P. Teixeira-Dias⁹⁴, J. J. Teoh¹⁵⁴, K. Terashi¹⁵², J. Terron⁹⁸

S. Terzo¹³, M. Testa⁵³, R. J. Teuscher^{154,q}, N. Themistokleous⁵², T. Theveneaux-Pelzer¹⁸, O. Thielmann¹⁶⁹, D. W. Thomas⁹⁴, J. P. Thomas²⁰, E. A. Thompson⁴⁸, P. D. Thompson²⁰, E. Thomson¹²⁷, E. J. Thorpe⁹³, Y. Tian⁵⁵, V. Tikhomirov^{37,m}, Yu. A. Tikhonov³⁷, S. Timoshenko³⁷, E. X.L. Ting¹, P. Tipton¹⁷⁰, S. Tisserant¹⁰¹, S. H. Tlou^{33g}, A. Tnourji⁴⁰, K. Todome^{23b,23a}, S. Todorova-Nova¹³², S. Todt⁵⁰, M. Togawa⁸², J. Tojo⁸⁸, S. Tokár^{28a}, K. Tokushuku⁸², R. Tombs³², M. Tomoto^{82,110}, L. Tompkins¹⁴², P. Tornambe¹⁰², E. Torrence¹²², H. Torres⁵⁰, E. Torró Pastor¹⁶¹, M. Toscani³⁰, C. Tosciri³⁹, D. R. Tovey¹³⁸, A. Traet¹⁶, I. S. Trandafir^{27b}, T. Trefzger¹⁶⁴, A. Tricoli²⁹, I. M. Trigger^{155a}, S. Trincaz-Duvoid¹²⁶, D. A. Trischuk¹⁶², B. Trocmé⁶⁰, A. Trofymov⁶⁶, C. Troncon^{70a}, L. Truong^{33c}, M. Trzebinski⁸⁵, A. Trzupek⁸⁵, F. Tsai¹⁴⁴, M. Tsai¹⁰⁵, A. Tsiamis¹⁵¹, P. V. Tsiarshka³⁷, S. Tsigaridas^{155a}, A. Tsirigotis^{151,ab}, V. Tsiskaridze¹⁴⁴, E. G. Tskhadadze^{148a}, M. Tsopoulou¹⁵¹, Y. Tsujikawa⁸⁶, I. I. Tsukerman³⁷, V. Tsulaia^{17a}, S. Tsuno⁸², O. Tsur¹⁴⁹, D. Tsybychev¹⁴⁴, Y. Tu^{64b}, A. Tudorache^{27b}, V. Tudorache^{27b}, A. N. Tuna³⁶, S. Turchikhin³⁸, I. Turk Cakir^{3a}, R. Turra^{70a}, P. M. Tuts⁴¹, S. Tzamarias¹⁵¹, P. Tzani¹⁰, E. Tzovara⁹⁹, K. Uchida¹⁵², F. Ukegawa¹⁵⁶, P. A. Ulloa Poblete^{136c}, G. Unal³⁶, M. Unal¹¹, A. Undrus²⁹, G. Unel¹⁵⁸, K. Uno¹⁵², J. Urban^{28b}, P. Urquijo¹⁰⁴, G. Usai⁸, R. Ushioda¹⁵³, M. Usman¹⁰⁷, Z. Uysal^{21b}, V. Vacek¹³¹, B. Vachon¹⁰³, K. O.H. Vadla¹²⁴, T. Vafeiadis³⁶, C. Valderanis¹⁰⁸, E. Valdes Santurio^{47a,47b}, M. Valente^{155a}, S. Valentinetti^{23b,23a}, A. Valero¹⁶¹, A. Vallier¹⁰¹, J. A. Valls Ferrer¹⁶¹, T. R. Van Daalen¹³⁷, P. Van Gemmeren⁶, S. Van Stroud⁹⁵, I. Van Vulpen¹¹³, M. Vanadia^{75a,75b}, W. Vandelli³⁶, M. Vandenbroucke¹³⁴, E. R. Vandewall¹²⁰, D. Vannicola¹⁵⁰, L. Vannoli^{57b,57a}, R. Vari^{74a}, E. W. Varnes⁷, C. Varni^{17a}, T. Varol¹⁴⁷, D. Varouchas⁶⁶, L. Varriale¹⁶¹, K. E. Varvell¹⁴⁶, M. E. Vasile^{27b}, L. Vaslin⁴⁰, G. A. Vasquez¹⁶³, F. Vazeille⁴⁰, T. Vazquez Schroeder³⁶, J. Veatch³¹, V. Vecchio¹⁰⁰, M. J. Veen¹¹³, I. Veliscek¹²⁵, L. M. Veloce¹⁵⁴, F. Veloso^{129a,129c}, S. Veneziano^{74a}, A. Ventura^{69a,69b}, A. Verbitskiy¹⁰⁹, M. Verducci^{73a,73b}, C. Vergis²⁴, M. Verissimo De Araujo^{81b}, W. Verkerke¹¹³, J. C. Vermeulen¹¹³, C. Vernieri¹⁴², P. J. Verschuur⁹⁴, M. Vessella¹⁰², M. L. Vesterbacka¹¹⁶, M. C. Vetterli^{141,d}, A. Vgenopoulos¹⁵¹, N. Viaux Maira^{136f}, T. Vickey¹³⁸, O. E. Vickey Boeriu¹³⁸, G. H.A. Viehhauser¹²⁵, L. Vignani^{63b}, M. Villa^{23b,23a}, M. Villaplana Perez¹⁶¹, E. M. Villhauer⁵², E. Vilucchi⁵³, M. G. Vincker³⁴, G. S. Virdee²⁰, A. Vishwakarma⁵², C. Vittori^{23b,23a}, I. Vivarelli¹⁴⁵, V. Vladimirov¹⁶⁵, E. Voevodina¹⁰⁹, F. Vogel¹⁰⁸, P. Vokac¹³¹, J. Von Ahnen¹³¹, E. Von Toerne²⁴, B. Vormwald³⁶, V. Vorobel¹³², K. Vorobev³⁷, M. Vos¹⁶¹, J. H. Vosseveld⁹¹, M. Vozak¹¹³, L. Vozdecky⁹³, N. Vranjes¹⁵, M. Vranjes Milosavljevic¹⁵, M. Vreeswijk¹¹³, R. Vuillemet³⁶, O. Vujanovic⁹⁹, I. Vukotic³⁹, S. Wada¹⁵⁶, C. Wagner¹⁰², W. Wagner¹⁶⁹, S. Wahdan¹⁶⁹, H. Wahlberg⁸⁹, R. Wakasa¹⁵⁶, M. Wakida¹¹⁰, V. M. Walbrecht¹⁰⁹, J. Walder¹³³, R. Walker¹⁰⁸, W. Walkowiak¹⁴⁰, A. M. Wang⁶¹, A. Z. Wang¹⁶⁸, C. Wang^{62a}, C. Wang^{62c}, H. Wang^{17a}, J. Wang^{64a}, P. Wang⁴⁴, R.-J. Wang⁹⁹, R. Wang⁶¹, R. Wang⁶, S. M. Wang¹⁴⁷, S. Wang^{62b}, T. Wang^{62a}, W. T. Wang⁷⁹, W. X. Wang^{62a}, X. Wang^{14c}, X. Wang¹⁶⁰, X. Wang^{62c}, Y. Wang^{62d}, Y. Wang^{14c}, Z. Wang¹⁰⁵, Z. Wang^{62d,51,62c}, Z. Wang¹⁰⁵, A. Warburton¹⁰³, R. J. Ward²⁰, N. Warrack⁵⁹, A. T. Watson²⁰, M. F. Watson²⁰, G. Watts¹³⁷, B. M. Waugh⁹⁵, A. F. Webb¹¹, C. Weber²⁹, M. S. Weber¹⁹, S. A. Weber³⁴, S. M. Weber^{63a}, C. Wei^{62a}, Y. Wei¹²⁵, A. R. Weidberg¹²⁵, J. Weingarten⁴⁹, M. Weirich⁹⁹, C. Weiser⁵⁴, C. J. Wells⁴⁸, T. Wenaus²⁹, B. Wendland⁴⁹, T. Wengler³⁶, N. S. Wenke¹⁰⁹, N. Wermes²⁴, M. Wessels^{63a}, K. Whalen¹²², A. M. Wharton⁹⁰, A. S. White⁶¹, A. White⁸, M. J. White¹, D. Whiteson¹⁵⁸, L. Wickremasinghe¹²³, W. Wiedenmann¹⁶⁸, C. Wiel⁵⁰, M. Wielers¹³³, N. Wieseotte⁹⁹, C. Wiglesworth⁴², L. A.M. Wiik-Fuchs⁵⁴, D. J. Wilbern¹¹⁹, H. G. Wilkens³⁶, D. M. Williams⁴¹, H. H. Williams¹²⁷, S. Williams³², S. Willocq¹⁰², P. J. Windischhofer¹²⁵, F. Winklmeier¹²², B. T. Winter⁵⁴, M. Wittgen¹⁴², M. Wobisch⁹⁶, A. Wolf⁹⁹, R. Wölker¹²⁵, J. Wollrath¹⁵⁸, M. W. Wolter⁸⁵, H. Wolters^{129a,129c}, V. W.S. Wong¹⁶², A. F. Wongel⁴⁸, S. D. Worm⁴⁸, B. K. Wosiek⁸⁵, K. W. Woźniak⁸⁵, K. Wraight⁵⁹, J. Wu^{14a,14d}, M. Wu^{64a}, S. L. Wu¹⁶⁸, X. Wu⁵⁶, Y. Wu^{62a}, Z. Wu^{134,62a}, J. Wuerzinger¹²⁵, T. R. Wyatt¹⁰⁰, B. M. Wynne⁵², S. Xella⁴², L. Xia^{14c}, M. Xia^{14b}, J. Xiang^{64c}, X. Xiao¹⁰⁵, M. Xie^{62a}, X. Xie^{62a}, J. Xiong^{17a}, I. Xiotidis¹⁴⁵, D. Xu^{14a}, H. Xu^{62a}, H. Xu^{62a}, L. Xu^{62a}, R. Xu¹²⁷, T. Xu¹⁰⁵, W. Xu¹⁰⁵, Y. Xu^{14b}, Z. Xu^{62b}, Z. Xu¹⁴², B. Yabsley¹⁴⁶, S. Yacoob^{33a}, N. Yamaguchi⁸⁸, Y. Yamaguchi¹⁵³, H. Yamauchi¹⁵⁶, T. Yamazaki^{17a}, Y. Yamazaki⁸³, J. Yan^{62c}, S. Yan¹²⁵, Z. Yan²⁵, H. J. Yang^{62c,62d}, H. T. Yang^{17a}, S. Yang^{62a}, T. Yang^{64c}, X. Yang^{62a}, X. Yang^{14a}, Y. Yang⁴⁴, Z. Yang^{62a,105}, W.-M. Yao^{17a}, Y. C. Yap⁴⁸, H. Ye^{14c}, J. Ye⁴⁴, S. Ye²⁹, X. Ye^{62a}, I. Yeletsikh³⁸, M. R. Yexley⁹⁰, P. Yin⁴¹, K. Yorita¹⁶⁶, C. J.S. Young⁵⁴, C. Young¹⁴², M. Yuan¹⁰⁵, R. Yuan¹⁰⁵, X. Yue^{62b,ah}, X. Yue^{63a}, M. Zaazoua^{35e}, B. Zabinski⁸⁵, E. Zaid⁵², T. Zakareishvili^{148b}, N. Zakharchuk³⁴, S. Zambito⁵⁶, J. Zang¹⁵², D. Zanzi⁵⁴, O. Zaplatilek¹³¹, S. V. ZeiBner⁴⁹, C. Zeitnitz¹⁶⁹, J. C. Zeng¹⁶⁰, D. T. Zenger Jr²⁶, O. Zenin³⁷, T. Ženiš^{28a}, S. Zenz⁹³, S. Zerradi^{35a}, D. Zerwas⁶⁶, B. Zhang^{14c}, D. F. Zhang¹³⁸, G. Zhang^{14b}, J. Zhang⁶, K. Zhang^{14a,14d}, L. Zhang^{14c}, R. Zhang¹⁶⁸, S. Zhang¹⁰⁵, T. Zhang¹⁵², X. Zhang^{62c}, X. Zhang^{62b}, Z. Zhang⁶⁶, H. Zhao¹³⁷, P. Zhao⁵¹, T. Zhao^{62b}, Y. Zhao¹³⁵, Z. Zhao^{62a}, A. Zhemchugov³⁸, Z. Zheng¹⁴², D. Zhong¹⁶⁰, B. Zhou¹⁰⁵, C. Zhou¹⁶⁸, H. Zhou⁷, N. Zhou^{62c}, Y. Zhou⁷, C. G. Zhu^{62b}, C. Zhu^{14a,14d}, H. L. Zhu^{62a}, H. Zhu^{14a}, J. Zhu¹⁰⁵, Y. Zhu^{62a}, X. Zhuang^{14a}, K. Zhukov³⁷, V. Zhulanov³⁷, N. I. Zimine³⁸, J. Zinsser^{63b}, M. Ziolkowski¹⁴⁰, L. Živković¹⁵, A. Zoccoli^{23b,23a}, K. Zoch⁵⁶, T. G. Zorbass¹³⁸, O. Zormpa⁴⁶, W. Zou⁴¹ and L. Zwalinski³⁶

(ATLAS Collaboration)

- ¹Department of Physics, University of Adelaide, Adelaide, Australia
²Department of Physics, University of Alberta, Edmonton AB, Canada
^{3a}Department of Physics, Ankara University, Ankara, Türkiye
^{3b}Division of Physics, TOBB University of Economics and Technology, Ankara, Türkiye
⁴LAPP, Univ. Savoie Mont Blanc, CNRS/IN2P3, Annecy, France
⁵APC, Université Paris Cité, CNRS/IN2P3, Paris, France
⁶High Energy Physics Division, Argonne National Laboratory, Argonne IL, USA
⁷Department of Physics, University of Arizona, Tucson AZ, USA
⁸Department of Physics, University of Texas at Arlington, Arlington TX, USA
⁹Physics Department, National and Kapodistrian University of Athens, Athens, Greece
¹⁰Physics Department, National Technical University of Athens, Zografou, Greece
¹¹Department of Physics, University of Texas at Austin, Austin TX, USA
¹²Institute of Physics, Azerbaijan Academy of Sciences, Baku, Azerbaijan
¹³Institut de Física d'Altes Energies (IFAE), Barcelona Institute of Science and Technology, Barcelona, Spain
^{14a}Institute of High Energy Physics, Chinese Academy of Sciences, Beijing, China
^{14b}Physics Department, Tsinghua University, Beijing, China
^{14c}Department of Physics, Nanjing University, Nanjing, China
^{14d}University of Chinese Academy of Science (UCAS), Beijing, China
¹⁵Institute of Physics, University of Belgrade, Belgrade, Serbia
¹⁶Department for Physics and Technology, University of Bergen, Bergen, Norway
^{17a}Physics Division, Lawrence Berkeley National Laboratory, Berkeley CA, USA
^{17b}University of California, Berkeley CA, USA
¹⁸Institut für Physik, Humboldt Universität zu Berlin, Berlin, Germany
¹⁹Albert Einstein Center for Fundamental Physics and Laboratory for High Energy Physics, University of Bern, Bern, Switzerland
²⁰School of Physics and Astronomy, University of Birmingham, Birmingham, United Kingdom
^{21a}Department of Physics, Bogazici University, Istanbul, Türkiye
^{21b}Department of Physics Engineering, Gaziantep University, Gaziantep, Türkiye
^{21c}Department of Physics, Istanbul University, Istanbul, Türkiye
^{21d}Istinye University, Sariyer, Istanbul, Türkiye
^{22a}Facultad de Ciencias y Centro de Investigaciones, Universidad Antonio Nariño, Bogotá, Colombia
^{22b}Departamento de Física, Universidad Nacional de Colombia, Bogotá, Colombia
^{23a}Dipartimento di Fisica e Astronomia A. Righi, Università di Bologna, Bologna, Italy
^{23b}INFN Sezione di Bologna, Italy
²⁴Physikalisches Institut, Universität Bonn, Bonn, Germany
²⁵Department of Physics, Boston University, Boston MA, USA
²⁶Department of Physics, Brandeis University, Waltham MA, USA
^{27a}Transilvania University of Brasov, Brasov, Romania
^{27b}Horia Hulubei National Institute of Physics and Nuclear Engineering, Bucharest, Romania
^{27c}Department of Physics, Alexandru Ioan Cuza University of Iasi, Iasi, Romania
^{27d}National Institute for Research and Development of Isotopic and Molecular Technologies, Physics Department, Cluj-Napoca, Romania
^{27e}University Politehnica Bucharest, Bucharest, Romania
^{27f}West University in Timisoara, Timisoara, Romania
^{28a}Faculty of Mathematics, Physics and Informatics, Comenius University, Bratislava, Slovak Republic
^{28b}Department of Subnuclear Physics, Institute of Experimental Physics of the Slovak Academy of Sciences, Kosice, Slovak Republic
²⁹Physics Department, Brookhaven National Laboratory, Upton NY, USA
³⁰Universidad de Buenos Aires, Facultad de Ciencias Exactas y Naturales, Departamento de Física, y CONICET, Instituto de Física de Buenos Aires (IFIBA), Buenos Aires, Argentina
³¹California State University, CA, USA
³²Cavendish Laboratory, University of Cambridge, Cambridge, United Kingdom
^{33a}Department of Physics, University of Cape Town, Cape Town, South Africa
^{33b}iThemba Labs, Western Cape, South Africa
^{33c}Department of Mechanical Engineering Science, University of Johannesburg, Johannesburg, South Africa
^{33d}National Institute of Physics, University of the Philippines Diliman (Philippines), South Africa
^{33e}University of South Africa, Department of Physics, Pretoria, South Africa
^{33f}University of Zululand, KwaDlangezwa, South Africa
^{33g}School of Physics, University of the Witwatersrand, Johannesburg, South Africa
³⁴Department of Physics, Carleton University, Ottawa ON, Canada
^{35a}Faculté des Sciences Ain Chock, Réseau Universitaire de Physique des Hautes Energies - Université Hassan II, Casablanca, Morocco

- ^{35b} *Faculté des Sciences, Université Ibn-Tofail, Kénitra, Morocco*
- ^{35c} *Faculté des Sciences Semlalia, Université Cadi Ayyad, LPHEA-Marrakech, Morocco*
- ^{35d} *LPMR Faculté des Sciences, Université Mohamed Premier, Oujda, Morocco*
- ^{35e} *Faculté des sciences, Université Mohammed V, Rabat, Morocco*
- ^{35f} *Institute of Applied Physics, Mohammed VI Polytechnic University, Ben Guerir, Morocco*
- ³⁶ *CERN, Geneva, Switzerland*
- ³⁷ *Affiliated with an institute covered by a cooperation agreement with CERN*
- ³⁸ *Affiliated with an international laboratory covered by a cooperation agreement with CERN*
- ³⁹ *Enrico Fermi Institute, University of Chicago, Chicago IL, USA*
- ⁴⁰ *LPC, Université Clermont Auvergne, CNRS/IN2P3, Clermont-Ferrand, France*
- ⁴¹ *Nevis Laboratory, Columbia University, Irvington NY, USA*
- ⁴² *Niels Bohr Institute, University of Copenhagen, Copenhagen, Denmark*
- ^{43a} *Dipartimento di Fisica, Università della Calabria, Rende, Italy*
- ^{43b} *INFN Gruppo Collegato di Cosenza, Laboratori Nazionali di Frascati, Italy*
- ⁴⁴ *Physics Department, Southern Methodist University, Dallas TX, USA*
- ⁴⁵ *Physics Department, University of Texas at Dallas, Richardson TX, USA*
- ⁴⁶ *National Centre for Scientific Research “Demokritos”, Agia Paraskevi, Greece*
- ^{47a} *Department of Physics, Stockholm University, Sweden*
- ^{47b} *Oskar Klein Centre, Stockholm, Sweden*
- ⁴⁸ *Deutsches Elektronen-Synchrotron DESY, Hamburg and Zeuthen, Germany*
- ⁴⁹ *Fakultät Physik, Technische Universität Dortmund, Dortmund, Germany*
- ⁵⁰ *Institut für Kern- und Teilchenphysik, Technische Universität Dresden, Dresden, Germany*
- ⁵¹ *Department of Physics, Duke University, Durham NC, USA*
- ⁵² *SUPA - School of Physics and Astronomy, University of Edinburgh, Edinburgh, United Kingdom*
- ⁵³ *INFN e Laboratori Nazionali di Frascati, Frascati, Italy*
- ⁵⁴ *Physikalisches Institut, Albert-Ludwigs-Universität Freiburg, Freiburg, Germany*
- ⁵⁵ *II. Physikalisches Institut, Georg-August-Universität Göttingen, Göttingen, Germany*
- ⁵⁶ *Département de Physique Nucléaire et Corpusculaire, Université de Genève, Genève, Switzerland*
- ^{57a} *Dipartimento di Fisica, Università di Genova, Genova, Italy*
- ^{57b} *INFN Sezione di Genova, Italy*
- ⁵⁸ *II. Physikalisches Institut, Justus-Liebig-Universität Giessen, Giessen, Germany*
- ⁵⁹ *SUPA - School of Physics and Astronomy, University of Glasgow, Glasgow, United Kingdom*
- ⁶⁰ *LPSC, Université Grenoble Alpes, CNRS/IN2P3, Grenoble INP, Grenoble, France*
- ⁶¹ *Laboratory for Particle Physics and Cosmology, Harvard University, Cambridge MA, USA*
- ^{62a} *Department of Modern Physics and State Key Laboratory of Particle Detection and Electronics, University of Science and Technology of China, Hefei, China*
- ^{62b} *Institute of Frontier and Interdisciplinary Science and Key Laboratory of Particle Physics and Particle Irradiation (MOE), Shandong University, Qingdao, China*
- ^{62c} *School of Physics and Astronomy, Shanghai Jiao Tong University, Key Laboratory for Particle Astrophysics and Cosmology (MOE), SKLPPC, Shanghai, China*
- ^{62d} *Tsung-Dao Lee Institute, Shanghai, China*
- ^{63a} *Kirchhoff-Institut für Physik, Ruprecht-Karls-Universität Heidelberg, Heidelberg, Germany*
- ^{63b} *Physikalisches Institut, Ruprecht-Karls-Universität Heidelberg, Heidelberg, Germany*
- ^{64a} *Department of Physics, Chinese University of Hong Kong, Shatin, N.T., Hong Kong, China*
- ^{64b} *Department of Physics, University of Hong Kong, Hong Kong, China*
- ^{64c} *Department of Physics and Institute for Advanced Study, Hong Kong University of Science and Technology, Clear Water Bay, Kowloon, Hong Kong, China*
- ⁶⁵ *Department of Physics, National Tsing Hua University, Hsinchu, Taiwan*
- ⁶⁶ *IJCLab, Université Paris-Saclay, CNRS/IN2P3, 91405, Orsay, France*
- ⁶⁷ *Department of Physics, Indiana University, Bloomington IN, USA*
- ^{68a} *INFN Gruppo Collegato di Udine, Sezione di Trieste, Udine, Italy*
- ^{68b} *ICTP, Trieste, Italy*
- ^{68c} *Dipartimento Politecnico di Ingegneria e Architettura, Università di Udine, Udine, Italy*
- ^{69a} *INFN Sezione di Lecce, Italy*
- ^{69b} *Dipartimento di Matematica e Fisica, Università del Salento, Lecce, Italy*
- ^{70a} *INFN Sezione di Milano, Italy*
- ^{70b} *Dipartimento di Fisica, Università di Milano, Milano, Italy*
- ^{71a} *INFN Sezione di Napoli, Italy*
- ^{71b} *Dipartimento di Fisica, Università di Napoli, Napoli, Italy*

- ^{72a}INFN Sezione di Pavia, Italy
^{72b}Dipartimento di Fisica, Università di Pavia, Pavia, Italy
^{73a}INFN Sezione di Pisa, Italy
^{73b}Dipartimento di Fisica E. Fermi, Università di Pisa, Pisa, Italy
^{74a}INFN Sezione di Roma, Italy
^{74b}Dipartimento di Fisica, Sapienza Università di Roma, Roma, Italy
^{75a}INFN Sezione di Roma Tor Vergata, Italy
^{75b}Dipartimento di Fisica, Università di Roma Tor Vergata, Roma, Italy
^{76a}INFN Sezione di Roma Tre, Italy
^{76b}Dipartimento di Matematica e Fisica, Università Roma Tre, Roma, Italy
^{77a}INFN-TIFPA, Italy
^{77b}Università degli Studi di Trento, Trento, Italy
⁷⁸Universität Innsbruck, Department of Astro and Particle Physics, Innsbruck, Austria
⁷⁹University of Iowa, Iowa City IA, USA
⁸⁰Department of Physics and Astronomy, Iowa State University, Ames IA, USA
^{81a}Departamento de Engenharia Elétrica, Universidade Federal de Juiz de Fora (UFJF), Juiz de Fora, Brazil
^{81b}Universidade Federal do Rio De Janeiro COPPE/EE/IF, Rio de Janeiro, Brazil
^{81c}Instituto de Física, Universidade de São Paulo, São Paulo, Brazil
^{81d}Rio de Janeiro State University, Rio de Janeiro, Brazil
⁸²KEK, High Energy Accelerator Research Organization, Tsukuba, Japan
⁸³Graduate School of Science, Kobe University, Kobe, Japan
^{84a}AGH University of Science and Technology, Faculty of Physics and Applied Computer Science, Krakow, Poland
^{84b}Marian Smoluchowski Institute of Physics, Jagiellonian University, Krakow, Poland
⁸⁵Institute of Nuclear Physics Polish Academy of Sciences, Krakow, Poland
⁸⁶Faculty of Science, Kyoto University, Kyoto, Japan
⁸⁷Kyoto University of Education, Kyoto, Japan
⁸⁸Research Center for Advanced Particle Physics and Department of Physics, Kyushu University, Fukuoka, Japan
⁸⁹Instituto de Física La Plata, Universidad Nacional de La Plata and CONICET, La Plata, Argentina
⁹⁰Physics Department, Lancaster University, Lancaster, United Kingdom
⁹¹Oliver Lodge Laboratory, University of Liverpool, Liverpool, United Kingdom
⁹²Department of Experimental Particle Physics, Jožef Stefan Institute and Department of Physics, University of Ljubljana, Ljubljana, Slovenia
⁹³School of Physics and Astronomy, Queen Mary University of London, London, United Kingdom
⁹⁴Department of Physics, Royal Holloway University of London, Egham, United Kingdom
⁹⁵Department of Physics and Astronomy, University College London, London, United Kingdom
⁹⁶Louisiana Tech University, Ruston LA, USA
⁹⁷Fysiska institutionen, Lunds universitet, Lund, Sweden
⁹⁸Departamento de Física Teórica C-15 and CIAFF, Universidad Autónoma de Madrid, Madrid, Spain
⁹⁹Institut für Physik, Universität Mainz, Mainz, Germany
¹⁰⁰School of Physics and Astronomy, University of Manchester, Manchester, United Kingdom
¹⁰¹CPPM, Aix-Marseille Université, CNRS/IN2P3, Marseille, France
¹⁰²Department of Physics, University of Massachusetts, Amherst MA, USA
¹⁰³Department of Physics, McGill University, Montreal QC, Canada
¹⁰⁴School of Physics, University of Melbourne, Victoria, Australia
¹⁰⁵Department of Physics, University of Michigan, Ann Arbor MI, USA
¹⁰⁶Department of Physics and Astronomy, Michigan State University, East Lansing MI, USA
¹⁰⁷Group of Particle Physics, University of Montreal, Montreal QC, Canada
¹⁰⁸Fakultät für Physik, Ludwig-Maximilians-Universität München, München, Germany
¹⁰⁹Max-Planck-Institut für Physik (Werner-Heisenberg-Institut), München, Germany
¹¹⁰Graduate School of Science and Kobayashi-Maskawa Institute, Nagoya University, Nagoya, Japan
¹¹¹Department of Physics and Astronomy, University of New Mexico, Albuquerque NM, USA
¹¹²Institute for Mathematics, Astrophysics and Particle Physics, Radboud University/Nikhef, Nijmegen, Netherlands
¹¹³Nikhef National Institute for Subatomic Physics and University of Amsterdam, Amsterdam, Netherlands
¹¹⁴Department of Physics, Northern Illinois University, DeKalb IL, USA
^{115a}New York University Abu Dhabi, Abu Dhabi, United Arab Emirates
^{115b}United Arab Emirates University, Al Ain, United Arab Emirates
^{115c}University of Sharjah, Sharjah, United Arab Emirates
¹¹⁶Department of Physics, New York University, New York NY, USA
¹¹⁷Ochanomizu University, Otsuka, Bunkyo-ku, Tokyo, Japan
¹¹⁸Ohio State University, Columbus OH, USA

- ¹¹⁹Homer L. Dodge Department of Physics and Astronomy, University of Oklahoma, Norman OK, USA
¹²⁰Department of Physics, Oklahoma State University, Stillwater OK, USA
¹²¹Palacký University, Joint Laboratory of Optics, Olomouc, Czech Republic
¹²²Institute for Fundamental Science, University of Oregon, Eugene, OR, USA
¹²³Graduate School of Science, Osaka University, Osaka, Japan
¹²⁴Department of Physics, University of Oslo, Oslo, Norway
¹²⁵Department of Physics, Oxford University, Oxford, United Kingdom
¹²⁶LPNHE, Sorbonne Université, Université Paris Cité, CNRS/IN2P3, Paris, France
¹²⁷Department of Physics, University of Pennsylvania, Philadelphia PA, USA
¹²⁸Department of Physics and Astronomy, University of Pittsburgh, Pittsburgh PA, USA
^{129a}Laboratório de Instrumentação e Física Experimental de Partículas - LIP, Lisboa, Portugal
^{129b}Departamento de Física, Faculdade de Ciências, Universidade de Lisboa, Lisboa, Portugal
^{129c}Departamento de Física, Universidade de Coimbra, Coimbra, Portugal
^{129d}Centro de Física Nuclear da Universidade de Lisboa, Lisboa, Portugal
^{129e}Departamento de Física, Universidade do Minho, Braga, Portugal
^{129f}Departamento de Física Teórica y del Cosmos, Universidad de Granada, Granada (Spain), Portugal
^{129g}Instituto Superior Técnico, Universidade de Lisboa, Lisboa, Portugal
¹³⁰Institute of Physics of the Czech Academy of Sciences, Prague, Czech Republic
¹³¹Czech Technical University in Prague, Prague, Czech Republic
¹³²Charles University, Faculty of Mathematics and Physics, Prague, Czech Republic
¹³³Particle Physics Department, Rutherford Appleton Laboratory, Didcot, United Kingdom
¹³⁴IRFU, CEA, Université Paris-Saclay, Gif-sur-Yvette, France
¹³⁵Santa Cruz Institute for Particle Physics, University of California Santa Cruz, Santa Cruz CA, USA
^{136a}Departamento de Física, Pontificia Universidad Católica de Chile, Santiago, Chile
^{136b}Millennium Institute for Subatomic physics at high energy frontier (SAPHIR), Santiago, Chile
^{136c}Instituto de Investigación Multidisciplinario en Ciencia y Tecnología, y Departamento de Física, Universidad de La Serena, Chile
^{136d}Universidad Andres Bello, Department of Physics, Santiago, Chile
^{136e}Instituto de Alta Investigación, Universidad de Tarapacá, Arica, Chile
^{136f}Departamento de Física, Universidad Técnica Federico Santa María, Valparaíso, Chile
¹³⁷Department of Physics, University of Washington, Seattle WA, USA
¹³⁸Department of Physics and Astronomy, University of Sheffield, Sheffield, United Kingdom
¹³⁹Department of Physics, Shinshu University, Nagano, Japan
¹⁴⁰Department Physik, Universität Siegen, Siegen, Germany
¹⁴¹Department of Physics, Simon Fraser University, Burnaby BC, Canada
¹⁴²SLAC National Accelerator Laboratory, Stanford CA, USA
¹⁴³Department of Physics, Royal Institute of Technology, Stockholm, Sweden
¹⁴⁴Departments of Physics and Astronomy, Stony Brook University, Stony Brook NY, USA
¹⁴⁵Department of Physics and Astronomy, University of Sussex, Brighton, United Kingdom
¹⁴⁶School of Physics, University of Sydney, Sydney, Australia
¹⁴⁷Institute of Physics, Academia Sinica, Taipei, Taiwan
^{148a}E. Andronikashvili Institute of Physics, Iv. Javakhishvili Tbilisi State University, Tbilisi, Georgia
^{148b}High Energy Physics Institute, Tbilisi State University, Tbilisi, Georgia
^{148c}University of Georgia, Tbilisi, Georgia
¹⁴⁹Department of Physics, Technion, Israel Institute of Technology, Haifa, Israel
¹⁵⁰Raymond and Beverly Sackler School of Physics and Astronomy, Tel Aviv University, Tel Aviv, Israel
¹⁵¹Department of Physics, Aristotle University of Thessaloniki, Thessaloniki, Greece
¹⁵²International Center for Elementary Particle Physics and Department of Physics, University of Tokyo, Tokyo, Japan
¹⁵³Department of Physics, Tokyo Institute of Technology, Tokyo, Japan
¹⁵⁴Department of Physics, University of Toronto, Toronto ON, Canada
^{155a}TRIUMF, Vancouver BC, Canada
^{155b}Department of Physics and Astronomy, York University, Toronto ON, Canada
¹⁵⁶Division of Physics and Tomonaga Center for the History of the Universe, Faculty of Pure and Applied Sciences, University of Tsukuba, Tsukuba, Japan
¹⁵⁷Department of Physics and Astronomy, Tufts University, Medford MA, USA
¹⁵⁸Department of Physics and Astronomy, University of California Irvine, Irvine CA, USA
¹⁵⁹Department of Physics and Astronomy, University of Uppsala, Uppsala, Sweden
¹⁶⁰Department of Physics, University of Illinois, Urbana IL, USA
¹⁶¹Instituto de Física Corpuscular (IFIC), Centro Mixto Universidad de Valencia - CSIC, Valencia, Spain
¹⁶²Department of Physics, University of British Columbia, Vancouver BC, Canada

¹⁶³*Department of Physics and Astronomy, University of Victoria, Victoria BC, Canada*

¹⁶⁴*Fakultät für Physik und Astronomie, Julius-Maximilians-Universität Würzburg, Würzburg, Germany*

¹⁶⁵*Department of Physics, University of Warwick, Coventry, United Kingdom*

¹⁶⁶*Waseda University, Tokyo, Japan*

¹⁶⁷*Department of Particle Physics and Astrophysics, Weizmann Institute of Science, Rehovot, Israel*

¹⁶⁸*Department of Physics, University of Wisconsin, Madison WI, USA*

¹⁶⁹*Fakultät für Mathematik und Naturwissenschaften, Fachgruppe Physik, Bergische Universität Wuppertal, Wuppertal, Germany*

¹⁷⁰*Department of Physics, Yale University, New Haven CT, USA*

^aAlso at Department of Physics, King's College London, London, United Kingdom.

^bAlso at Institute of Physics, Azerbaijan Academy of Sciences, Baku, Azerbaijan.

^cAlso at Lawrence Livermore National Laboratory, Livermore, USA.

^dAlso at TRIUMF, Vancouver BC, Canada.

^eAlso at Department of Physics, University of Thessaly, Greece.

^fAlso at Physics Department, An-Najah National University, Nablus, Palestine.

^gAlso at Department of Physics, University of Fribourg, Fribourg, Switzerland.

^hAlso at University of Colorado Boulder, Department of Physics, Colorado, USA.

ⁱAlso at Department of Physics and Astronomy, University of Louisville, Louisville, KY, USA.

^jDeceased.

^kAlso at Department of Physics, Westmont College, Santa Barbara, USA.

^lAlso at Departament de Física de la Universitat Autònoma de Barcelona, Barcelona, Spain.

^mAlso Affiliated with an institute covered by a cooperation agreement with CERN.

ⁿAlso at The Collaborative Innovation Center of Quantum Matter (CICQM), Beijing, China.

^oAlso at Department of Physics, Ben Gurion University of the Negev, Beer Sheva, Israel.

^pAlso at Università di Napoli Parthenope, Napoli, Italy.

^qAlso at Institute of Particle Physics (IPP), Canada.

^rAlso at Bruno Kessler Foundation, Trento, Italy.

^sAlso at Borough of Manhattan Community College, City University of New York, New York NY, USA.

^tAlso at Department of Financial and Management Engineering, University of the Aegean, Chios, Greece.

^uAlso at Centro Studi e Ricerche Enrico Fermi, Italy.

^vAlso at Department of Physics, California State University, East Bay, USA.

^wAlso at Institutio Catalana de Recerca i Estudis Avancats, ICREA, Barcelona, Spain.

^xAlso at University of Chinese Academy of Sciences (UCAS), Beijing, China.

^yAlso at Yeditepe University, Physics Department, Istanbul, Türkiye.

^zAlso at Institute of Theoretical Physics, Ilia State University, Tbilisi, Georgia.

^{aa}Also at CERN, Geneva, Switzerland.

^{ab}Also at Hellenic Open University, Patras, Greece.

^{ac}Also at Center for High Energy Physics, Peking University, China.

^{ad}Also at The City College of New York, New York NY, USA.

^{ae}Also at Department of Physics, California State University, Sacramento, USA.

^{af}Also at Département de Physique Nucléaire et Corpusculaire, Université de Genève, Genève, Switzerland.

^{ag}Also at Institut für Experimentalphysik, Universität Hamburg, Hamburg, Germany.

^{ah}Also at Department of Physics and Astronomy, Michigan State University, East Lansing MI, USA.